A *KCNQ2* variant causing Early Onset Epileptic Encephalopathy increases spontaneous network-driven activity and excitability of pyramidal cells in the layer II/III and V of the motor cortex during a limited period of development

Najoua Biba[1], Marie Kurz[1], Laurent Villard[2], Mathieu Milh[2,3], Hélène Becq[1] and Laurent Aniksztejn[1*]

1) INSERM UMR1249, INMED, Aix-Marseille University, Marseille, France
2) Aix-Marseille University, INSERM, MMG, , Marseille, France
3) Department of Pediatric Neurology, La Timone Children's Hospital, Marseille, France

* : Correspondance : Laurent Aniksztejn : INMED-INSERM UMR1249, Parc scientifique de Luminy, 163 route de Luminy, 13009 Marseille, France. E-mail :laurent.aniksztejn@inserm.fr

Number of figures:10; Number of tables : 2

Running title: A *KCNQ2* variant alters Layer II/III and V pyramidal cells excitability

Key words: KCNQ2, Kv7.2 channels, Epileptic encephalopathy, development, intrinsic properties, network activity

Summary

De novo variants in the *KCNQ2* gene encoding the Kv7.2 subunit of the voltage-gated potassium Kv7/M channel are the main cause of Early Onset Epileptic Encephalopathy (EOEE) with suppression burst suggesting that this channel plays an important role for proper brain development. Functional analysis of these variants in heterologous cells has shown that most of them are loss of function leading to a reduction of M current. However the cellular mechanism of the neuronal network dysfunctionning is still not known. Here we characterized the electrophysiological properties of developing pyramidal cells of the layer II/III and V and analyzed spontaneous synaptic activity in these layers in motor cortical slices obtained from a recently generated heterozygous knock-in mouse harboring the loss-of-function pathogenic p.T274M variant. Experiments were performed on animals aged one week, three weeks and four-five weeks, and the results were compared with those of pyramidal cells recorded in slices from wild-type mice untreated or treated with the Kv7 channel blocker XE-991. We showed that the variant led to a hyperexcitability of pyramidal cells of layer II/III in cortical slices from animal aged 1 week and 3 weeks and to a level that was similar to the effect of XE-911. In layer V the impact of the variant was observed in slices from animal aged 3 weeks but not earlier and to a level that was lower to the effect of XE-991. However, in cortical slices from animal aged 4-5 weeks electrophysiological properties of pyramidal cells of layers II/III and V were no more affected by the variant but still sensitive to XE-991. The recovery of the electrophysiological responses in knock-in animals was associated with a slight but significant distal shift of the axonal initial segment (AIS) from the soma of pyramidal cells of layer II/III and V. Recordings of spontaneous synaptic activity in these layers revealed the presence of recurrent GABAergic network activities (RGNA) that were mainly observed during the three first postnatal weeks of life and which occurrence and frequency were increased in pyramidal cells of the layer II/III but not of the layer V of the knock-in mouse. There were no significant differences in synaptic activities mediated by GABA and glutamate receptors in cortical slices from animal aged 4-5 weeks. Together our data provided evidences that the heterozygous p.T274M variant impacts the activity of pyramidal cells and probably of Gabaergic interneurons during a limited period of development. Our data also indicated that neurons of the layer II/III are more sensitive to the variant than those located in the layer V in terms of age of onset, neuronal firing and spontaneous synaptic activities. Moreover our data suggest that a compensatory mechanism might take place in the knock-in mice aged 4-5 weeks allowing the recovery of control activity at cellular and network levels and which is associated with a slight displacement of the AIS. Thus, the effect of the variant on neuronal activity is developmentally regulated and is reminiscent to some characteristics of *KCNQ2*-related EOEE.

Introduction

Channelopathies represent one of the major causes of neurological disorders including epileptic and developmental encephalopathies (EE), a group of severe and intractable diseases that associates severe epilepsy with a rapid deterioration of cognitive/sensory and motor functions. Among dozens of genes encoding for ion channels, *KCNQ2* which encodes the Kv7.2 subunits of Kv7 channels is probably the most frequently gene associated with neonatal onset epileptic encephalopathies (Weckhuysen et al., 2012; Kato et al., 2013; Milh et al., 2013; Allen et al., 2014; McTague et al., 2016; Allen et al., 2020, see also http://www.rikee.org/). This severe and intractable disease is characterized by seizures starting during the first days of life and a highly abnormal EEG, often showing a suppression-burst pattern (Ohtahara and Yamatogi, 2003).
Kv7.2 is one of the four subunits identified in the central nervous system (Kv7.2, 3, 4, 5) that are encoded by four *KCNQ* genes (*KCNQ2-5*). Each subunit consists of six transmembrane segments (S) with a voltage-sensor (S1-S4) domain and a pore domain (S5-P-S6) (Jentsch, 2000; Delmas and Brown, 2005). These subunits are abundant at axon initial segment (AIS), nodes of Ranvier, co-clustered with Nav channels, and synaptic terminals. There are less expressed at the soma but they are absent in dendrites of cortical pyramidal cells while in cortical interneurons these channels are detected in these subcellular regions (Devaux et al. 2004; Lawrence et al. , 2006; Battefeld et al., 2014; Huang and Trussell , 2011; Martinello et al., 2019).

Functional Kv7 channels are composed of homomeric or heteromeric assemblies of 4 subunits including Kv7.2/Kv7.3 in many cortical neurons and giving rise to the M current (Wang et al. 1998; Battefeld et al., 2014; Soh et al., 2014). M current is slowly activating and non-inactivating potassium current activating at subthreshold range of membrane potentials and which controls different aspects of neuronal excitability (Storm 1990; Brown and Passmore 2009). Thus, Kv7 channels control the resting membrane potential at the AIS and in terminals and spike threshold (Yue and Yaari, 2006; Shah et al., 2008; Hu and Bean 2018, Huang and Trussell, 2011; Martinello et al., 2019). At nodes of Ranvier, these channels increase the availability of Na^+ channels and thus the amplitude of the propagating action potential (Battefeld et al., 2014). At synaptic terminals Kv7 channels can control transmitter release (Vervaeke et al., 2006; Huang and Trussell, 2011; Martinello et al., 2019). Kv7 channels also reduce spike afterdepolarization, and mediate in some cells the medium afterhyperpolarization (mAHP) and contribute to the slow AHP (sAHP) (Storm, 1990; Gu et al., 2005; Yue and Yaari 2006). Thus, Kv7 channels serve as a brake for neuronal firing. These channels also influence excitatory synaptic potential integration (Hu et al., 2007; Shah et al., 2011) and contribute also to the slow substhreshold resonance of cortical neurons at theta frequency (4-7 Hz), oscillations that are important for synaptic plasticity, learning and memory (Hu et al. 2002).

Although the function of Kv7 channels and of the different subunits on neuronal properties is now well documented and deduces from the action of blockers, gene knock-out or specific subunits

deletion (Brown and Passmore, 2009; Peters et al. 2015; Soh et al.,2014, 2018; Fidzinski et al., 2015; Greene and Hoshi, 2017), the relationship between Kv7.2 variants and neurological disorders is still poorly understood. Functional consequences of variants in the *KCNQ2* gene associated to EOEE have widely been analyzed in heterologous cells. These study have shown that most of the variants are loss of function reducing M current carried by heteromeric channels from a moderate level (~25 %) to a strong level (>50%) (Miceli et al. 2013; Ohran et al., 2014; Abidi et al., 2015; Allen et al., 2020). This is notably the case of the p.T274 M variant (c.821C>T in the *KCNQ2* gene). This variant localized in the P loop between the segment S5 and the segment S6 of the pore domain exerts a dominant negative effect on wild type subunit reducing current amplitude by 60% in a configuration that mimics patient's situation and without any effects on the conductance-voltage relationship, protein production and membrane expression (Orhan et al., 2014). A recent study performed on neurons derived from human pluripotent stem cells shown that excitatory cells carrying the p.T274M variant develop intrinsic and network hyperexcitability progressively that was associated with an increase in the amplitude of the fast afterhyperpolarisation mediated by BK channels (Simkin et al., 2019). More recently, a knock-in mouse carrying the heterozygous p.T274M variant has been generated, the phenotype of which was reminiscent of some characteristics observed in EOEE patients (Milh et al., 2020). In particular, they have cognitive impairment and develop spontaneous seizures. Thus, this knock-in mouse could represent a good model to better understand how a Kv7.2 pathogenic variant alters cortical network functioning and ultimately at designing pharmacological options. Here, as a first step, we recorded pyramidal cells located in the layers II/III and V in developing motor cortical slices from this knock-in mouse and analyzed their electrophysiological properties and spontaneous synaptic activities. We wondered: - if the variant altered pyramidal cell excitability and spontaneous synaptic activities; -, if so, how this impact evolved during development and; - if the effect of the variant is equivalent in the different layers of the motor cortex.

Material and methods

Animals and genotyping

All experiments were carried out in accordance with the European Communities Council Directive of September 22, 2010 (2010/63/UE) related to laboratory animals used for research purposes. Experiments were performed on male and female postnatal day 7 (PND 7) to post-natal day 35 old 129Sv mice, housed in a temperature-controlled environment with a 12 light/dark cycle and free access to food and water (INMED animal facilities).

The generation of heterozygous *KCNQ2*$^{WT/T274M}$ knock-in mice and genotyping protocols have been described in a previous paper by Milh et al. (2020). Briefly, mice were genotyped by PCR. The following two primers were included in the PCR: A common forward primer (5'-

CTTGATCTTGTCCCCTGACTTGGTAGG-3') and a common reverse primer (5'-CCTAACATCTCCAGAGTAGGAAGGTGCG-3'). The primers amplified a 603 bp wild-type fragment and/or a 688 bp mutant fragment (Figure 1).

Slice preparation

Experiments were performed on pyramidal neurons located in the layers II/III and V of motor cortical slices.

Mice were euthanized by decapitation. The brain was rapidly removed and placed in an oxygenated ice-cold choline solution containing (in mM): 132.5 choline chloride, 2.5 KCl, 0.7 $CaCl_2$, 3 $MgCl_2$, 1.2 NaH_2PO_4, 25 $NaHCO_3$ and 8 glucose; oxygenated with 95% O_2 and 5% of CO_2. Coronal slices(300 µm-thick) containing the 2 interconnected hemispheres were cut using a vibratome (Leica VT1200S; Leica Microsystems, Germany) in ice-cold choline solution oxygenated with 95% O_2 and 5% of CO_2. Before recording, slices were incubated in an artificial cerebrospinal fluid (ACSF) solution with the following composition (in mM): 125 NaCl, 3.5 KCl, 2 $CaCl_2$, 1.3 $MgCl_2$, 1.25 NaH_2PO_4, 26 $NaHCO_3$ and 10 glucose equilibrated at pH 7.4 with 95% O_2 and 5% CO_2 at 34 °C for 20 min and then at room temperature (22–25 °C) for at least 1 h to allow recovery. For the recordings, slices were placed into the recording chamber where they were fully submerged and superfused with oxygenated ACSF solution at 34-35 °C at a rate of 5 ml/min.

Electrophysiology

Pyramidal cells of the layer II/III and V were recorded under visual control with a Zeiss Axioscope 2FS microscope in cell-attached and whole cell configurations using borosilicate glass capillaries (GC 150F-15). For recordings in current-clamp mode, patch-pipettes were filled with a solution containing (in mM): 140 $KMeSO_4$, 6 NaCl, 10 HEPES, 1 $MgCl_2$, 4 Mg-ATP, 0.4 Na_2-GTP. The pH was adjusted to 7.35 with KOH. The resistance of the pipettes was of 5-6 MΩ. For recordings in voltage-clamp mode, patch pipettes were filled with a solution containing (in mM): 120 Cs-gluconate, 10 CsCl, 10 HEPES, 4 Mg-ATP, 0.4 Na_2-GTP. The pH was adjusted to pH 7.35 with CsOH. The resistance of the pipettes was of 6-7 MΩ.

All reported potential values were corrected for the liquid junction potential, calculated to be ~2 mV with the $KMeSO_4$ pipette solution and ~15 mV with the Cs-gluconate filled pipette solution. Resting membrane potential was determined in current clamp as the potential upon break-in, before any current injection. Action potential (AP) threshold was defined as the membrane potential at which the rate of depolarization is maximal. All measurements were filtered at 3 KHz using an EPC10 amplifier (HEKA Electronik, Germany) and sampled at 10 kHz. Data were analyzed off-line using Clampfit (Molecular Devices), miniAnalysis (Synaptosoft), Origin 9 (Origin Lab), Prism 6 software (GraphPad).

Only cells with a stable resting membrane potential more negative than -60 mV were used in this study. All measurements in current-clamp mode were performed from a membrane potential of -70 mV (-72 with LJP correction), and if necessary, current was injected during the experiment to keep this value constant.

To calculate the membrane input resistance (Rm), voltage responses to the injection of five depolarizing and hyperpolarizing current steps, with an increment of +/-5 pA and applied during 500 msec ,were fit with a linear function to yield the slope value.

To calculate the membrane time constant (τ_m), the voltage response to the injection of a hyperpolarizing current step of -20 pA for 500 msec was fitted with a single exponential function (Origin 9) to yield the tau value. Membrane capacitance (Cm) was then calculated according to the equation $C_m = \tau_m/R_m$.

Action potentials were elicited by injection of short 10 msec and long 1 sec depolarizing current steps of 20 to 300 pA (increment of 20 pA) in pyramidal cells from animal aged one week and of 50-750 pA (increment 50 pA) from older animals. Currents injected by a slow ramp protocol were of 300 pA and 500 pA applied in 10 sec in pyramidal cells from animal aged one week and from older animals respectively.

Immunohistochemistry

Mice were transcardially perfused with the Antigenfix(dipath) in 3%, Brains were removed and post fixed 30min in 3% Antigenfix, watched 4h in PBS and stored in 20% sucrose 24h to 48h then frozen in the OCT (tissuetek Sakura) cooled in the dry ice. Serial coronal sections (20µm) encompassing the motor cortex were cut in the cryostat, slide mounted ant stored at -20°C.

Sections were blocked with a solution of PBS containing 0.3% triton and 1% NGS for 1h; antibodies were diluted in the same solution. Sections were incubated at 4°C overnight with rabbit anti NeuN (1: 500; Millipore), Mouse anti AnkyrinG (1:500, Neuromab) antibodies. Sections were watched (3x10min) in PBS 1% and incubated in Alexa goat anti rabbit 488(1:500) and Alexa goat anti mousse 555(1:500) secondary antibodies for 2h at room temperature. Then there was watched (2x10min) in PBS1% and incubated 10min with Hoechst (1:1000) diluted in PBS before a last watch in PBS and mounting in fluoromount-G™ .

Slices were viewed using a confocal microscope SP5-X (Leica, Germany). Z stacks of cortical neurons of layers II/III and V were acquired using a 63x oil objective. The measurement of the axonal initial segment (AIS) length and of the distance AIS-Soma distance was performed with neurolucida.

Statistics

Data are represented as means ± S.E.M. Student's t-test was used to compare means of two groups when the data's distribution was normal. When the normality test failed, we used the non-parametric Mann– Whitney test for two independent samples. Statistical analysis was performed using Graphpad Prism software. ns: not significant; *p < 0.05; **p <0.01; and ***p < 0.001.

Results

The p.T274M variant affects the excitability of pyramidal cells of the layer II/III during a transitory period of development .

Pyramidal cells located in the layer II/III of the motor cortex were recorded in slices using patch-clamp technic and carried out at three periods of development from mice aged one week (postnatal day 7-9, PND7-9), three weeks (PND 19-21) and 4-5 weeks (PND28-35). The properties of the cells obtained from wild type mice (*KCNQ2*$^{WT/WT}$, hereinafter referred to as "wild type cells") and from heterozygous knock-in *KCNQ2* mutant mice carrying the p.T274M variant (*KCNQ2*$^{WT/T274M}$, hereinafter referred to as "mutant cells") were compared. Furthermore, since the p.T274M mutation exerts a loss of function effect on Kv7/M channels activity in heterologous systems (Orhan et al., 2014), we also analyzed the action of the potent Kv7/M channels blocker XE-991 (20 µM) on pyramidal cells properties of wild type mice to see if the variant and the blocker had similar consequences. For this purpose, slices obtained from *KCNQ2*$^{WT/WT}$ mice were continuously superfused with the blocker (*KCNQ2*$^{WT/WT}$ in XE-991, hereinafter referred to as "XE-991 treated wild-type cells"). All recordings were performed in presence of gabazine (5 µM) to block $GABA_A$ receptors, NBQX (10 µM) to block AMPA/kainate receptors and D-APV (40 µM) to block NMDA receptors.

At PND7-9, in cell-attached configuration, cells of the layer II/III recorded in the three groups of slices were silent, there was not any spontaneous discharge in wild type cells recorded either in absence or in presence of XE-991, and in mutant cells (n = 16,11, 15 cells respectively; figure 2Aa). Therefore the dysfunction of M channels did not lead to the excitation of pyramidal cells at their true resting membrane potential. In whole-cell configuration, neither the mutation nor XE-991 had any effects on cell capacitance (Cm), membrane time constant (τ_m), and resting membrane potential (Vm) (table 1). However, the input resistance was higher and the current threshold to elicit a single action potential (AP) by short 10 msec depolarizing current steps, lower in mutant cells or in XE-991 treated wild-type cells compared to wild type cells (table 1). Moreover, the action potential (AP) membrane threshold was also significantly more hyperpolarized in the two former groups of cells whereas the amplitude, overshoot, halfwidth of the AP were unaffected (table 1). We then analyzed the neuronal discharge elicited by the injection of long 1 sec depolarizing current steps (from 20 to 300 pA). We quantified the number of AP, the frequency of the discharge during the first 200 msec of the steps

(initial frequency) and during the last 200 msec of the steps (final frequency). There were more AP in both mutant cells and XE-991 treated wild-type cells compared to wild-type cells for current steps below 150 pA but their number were similar or reduced for stronger current steps (Figure 2Ab,c). This was accompanied by a significant increase of the initial and final frequencies although for the latter parameter this increase was significant for current steps up to 100 pA. In fact, in both mutant cells and XE-991 treated wild type cells, the discharge was transient for steps above 120-160 pA whereas it was more sustained in wild-type cells (figure 2Ac). This was likely the consequence of the strong resistance of the 2 former groups of cells leading to a much larger depolarization produced by injection of current steps and to the progressive inactivation of voltage-gated Na^+ channels.

We next examined the response of the cells to the injection of a slow ramp of current of 300 pA applied in 10 sec. This procedure should facilitate the inactivation of several voltage-gated potassium channels and reveal much better the action of Kv7 channels which do not inactivate. Several parameters of the response were analyzed. These included the measurement of the chord resistance between -72 mV and the action potential threshold (R_{Chord}), the current injected required to evoke the first action potential ($I_{threshold}$), the number of AP, the initial frequency during the first second of the discharge. All of these parameters were significantly affected in the same direction by the variant or following the inhibition of Kv7 channels (figure 3A). Compared to wild type cells, the current threshold of both mutant cells and of XE-991 treated wild type cells was decreased, the AP membrane threshold more hyperpolarized (only for XE-991 treated cells), the initial frequency of the discharge was increased but the total number of AP was less due to a larger depolarization and the inactivation of voltage-gated Na^+ channels. Thus, the variation in the membrane potential produced by the injection of a ramp of current was of 47 ± 2.8 mV in wild type cells (n = 16), it was of 55.4 ± 2.9 mV in XE-991 treated wild-type cells (n = 11 cells) and of 57.8 ± 1.1 mV in mutant cells (n = 15 cells). Therefore, at the end of the first postnatal week of life, the variant or the inhibition of M channels had same consequences on the electrophysiological properties of pyramidal cells of the layer II/III. Both make cells more excitable in response to the injection of steps or a ramp of current but up to a certain range of current injected.

At PND19-21, wild-type pyramidal cells (n = 14 cells) had twice higher capacitance, twice lower input resistance and faster membrane time constant than at PND7-9 (table 1). Moreover, the current threshold to elicit an AP by the injection of steps or ramp of current was higher. Most of consequences of the variant and of XE-991 described at PND7-9 were maintained at three weeks. Like at PND7-9, in cell-attached configuration, the variant or the presence of the blocker did not lead pyramidal cells to spontaneously fire AP (n = 15 and 15 respectively, data not shown). In whole cell configuration, even if the variant or the M channel blocker had no more effect on input resistance measured around rest (table 1), the responses of the cells to the injection of steps (50-750 pA) or to a ramp of current (500 pA in 10sec) were similarly and significantly increased compared to the

responses of wild type cells (figures 2B, 3B). The excitability of pyramidal cells in these 2 former groups of cells was significantly enhanced compared to wild type cells and observed for a much larger range of current injected at PND7-9.

At PND28-35, the excitability of wild type pyramidal cells was higher than at PND19-21. These cells generated more AP in response to the injection of steps or a ramp of current at 4-5 weeks than at three weeks (n = 19 and 14 cells respectively). The number of AP elicited by these 2 procedures was affected neither by the mutation nor by XE-991 (n = 18 and 19 cells respectively). However, while the variant had no more significant effects on all of the parameters analyzed, in contrast, XE-991 treated wild type cells had a significant more depolarized resting membrane potential, higher input resistance and the current threshold to elicit a single action potential by injection of a short current step, lower (table 1). Moreover, XE-991 had still consequences on the initial frequency of the discharge which like at PND19-21 was stronger in the presence of the blocker than in its absence (figures 2C,3C). XE-991 also continued to affect the excitability of neurons and in particular the response of pyramidal cells to the injection of a slow ramp of current which the blocker altered in the same way than as in cells recorded at PND19-21.

Therefore, while the effect of XE-991 on the pyramidal cells of the layer II/III was maintained from the first end to the fifth postnatal week of life at least, the action of the variant on neuronal excitability was limited to the three first postnatal weeks of life.

Pyramidal cells of the layer V are impacted at a latter developmental stage by the variant than in the layer II/III but also during a restricted period of development

We next wondered if the variant and XE-991 impacted the excitability of pyramidal cells of other layers of the motor cortex and if these cells presented the same developmental sensitivity than described in the layer II/III. We recorded pyramidal cells of the layer V and performed same experiments than did in the layer II/III.

First, in cell-attached configuration wild-type cells, XE-991 treated wild type cells and mutant pyramidal cells of the layer V recorded from PND7 to PND35 were silent (data not shown).

In whole-cell configuration, at PND7-9, compared to pyramidal cells of the layer II/III, wild type pyramidal cells of the layer V had higher input resistance and lower rheobase (n = 15 cells, table 2). Furthermore, the number of AP generated by injection of current steps and their initial frequency were also higher for currents up to 220 pA and up to 160 pA respectively (Figure 4A,B). The responses of the cells of the upper and deep layers to the injection of a slow ramp of current were not significantly different (figures, 3A, 5A). At latter developmental stages, the responses of the cells of the layer V to the injection of steps or ramp of current were also highly comparable to the responses of the cells of the layer II/III. However they presented some differences in the sensitivity to XE-991 and to the

variant. In particular at PND7-9, cells of the layer V were affected neither by the variant (n = 15 cells) nor by the Kv7 channel blocker (n = 11 cells, table 2 and figures 4A,B, 5A). At PND19-21, the variant increased the number of AP elicited by injection of current steps and final frequency as it did in the layer II/III but had no effect on any parameters of the response analyzed and evoked by the injection of a ramp of current (n= 14 wild type cells; n = 15 mutant cells, figures 4A,C, 5B). XE-991 increased the input resistance of the cells and decreased the current threshold (table 2). The blocker also exerted a much powerful effect than did by the variant on neuronal discharge and initial frequency and also affected strongly the responses evoked by the injection of a ramp of current (n = 14 cells). At PND28-35, like for pyramidal cells of the layer II/III, the variant had no more consequences on cells of the layer V whereas XE-991 increased the number and the initial frequency of AP evoked by current steps and affected significantly most of the parameters of the responses elicited by the injection of a ramp of current (n = 16 wild type cells, n = 14 XE-991 treated wild type cells, n = 15 mutant cells, figures 4A,D, 5C).

Together these data showed that both the variant and XE-991 increased the excitability of pyramidal cells of the layer V but at a latter developmental stage than pyramidal cells of the layer II/III. In addition, like for pyramidal cells of the layer II/III, the variant alters the excitability of the cells until the third postnatal week of life. These data suggested that some compensatory mechanisms developed with time which reduced the impact of the variant on neuronal excitability.

Slight distal shift of the axonal initial segment of pyramidal cells of the motor cortex from *KCNQ2*$^{WT/T27M}$ mice aged 4-5 weeks.

Several studies have reported that the structure of the axonal initial segment (AIS) is highly plastic and can change in response to chronic alteration in neuronal activity (Kuba et al., 2010; Grubb and Burrone, 2010; Adachi et al., 2015; Wefelmeyer et al., 2016; Lezmy et al., 2017; Engelhardt et al., 2019). It has been proposed that these changes may contribute to normalize neuronal excitability. We wondered if a change in the length and the localization with respect to the soma of the AIS occurred at 4-5 weeks in mutant pyramidal cells of the layer II/III and V. For this purpose we performed immunostaining experiments and used confocal microscopy and Neurolucida for the measurements. The AIS were stained using α-ankyrin G antibody and cell bodies were stained using NeuN antibody (see methods). The staining of ankyrin G of wild-type pyramidal cells of the layers II/III and V showed that the distance between the soma from the AIS was very small, less than 1 µm, giving even the impression that the AIS was in close contact with the soma. This distance was more pronounced in mutant mice. There was a slight but significant distal shift of the AIS from the soma. This shift was not associated with a change in the length of the AIS (figures 6A, 7C). We performed same measurements at PND7-9 and PND 19-21 to determine if this shift was developmentally regulated. We did not observed a difference in the AIS-soma distance between wild-type and mutant cells of the

layer II/III and V at these two developmental periods (figures 6B,C, 7A,B). There were no differences in the length of the AIS of both pyramidal cells of the layer II/III and V from wild type and mutant mice.

Therefore a form of AIS plasticity occurred at the same developmental period than the recovery of control electrophysiological activity of pyramidal cells.

The p.T274M mutation increases spontaneous network-driven events in the layer II/III but not in layer V

We next analyzed spontaneous synaptic activity mediated by GABA and glutamate receptors at the same 3 developmental periods in both layer II/III and V in motor cortical slices from *KCNQ2*$^{WT/WT}$ and *KCNQ2*$^{WT/T274M}$ mice. For this purpose pyramidal cells located in these layers were recorded in both cell-attached configuration and in whole-cell in voltage clamp mode using patch pipettes filled with a Cs-gluconate solution (see methods). Postsynaptic currents mediated by $GABA_A$ receptors (GABAR-PSCs) were recorded at 0 mV, the reversal potential of glutamate, while those mediated by glutamate receptors (GluR-PSCs) were recorded at the reversal potential of GABA estimated ~-70 mV in our recording conditions.

In cell-attached configuration, we did not detected spontaneous action potentials in wild-type and mutant cells of layers II/III and V recorded between PND7 to PND 35 (figure 8A). Cells were still silent at their true resting membrane potential even in the absence of GABA and glutamate receptors antagonists although some "ondulation" of the current could be observed in some cells (see figure 8B, for example). In whole-cell configuration spontaneous postsynaptic events recorded in both populations of cells and at the three developmental periods were mainly mediated by $GABA_A$ receptors which frequency was 2 to 4 times higher than GluR-PSCs. In addition, the activity recorded at 0 mV included recurrent outward currents with a magnitude of few hundreds of pA and lasting between 0.5-2 sec (figure 8A,B, 9A). These large events were network activities resulting from the periodic summation of GABAergic postsynaptic currents. Indeed: i) their frequency did not change with the membrane potential; ii) they reversed polarity at the reversal potential of $GABA_A$ receptors; iii) they were insensitive to NBQX/APV (n = 4/4 cells); iv) they were fully blocked by gabazine (n = 4/4 cells) (figure 8A,B). These recurrent activities (Recurrent GABAergic Network Activity, RGNA) were more often observed in wild-type pyramidal cells of the layer II/III than of the layer V and were mainly recorded until PND19-21. They were absent in cells from mice aged 4-5 weeks (figures 9, 10).

At PND7-9, RGNA were recorded in 17/17 cells (3 animals) of the layer II/III, occurring at frequency ranging between 0.05 to 0.33 Hz and in 11/14 of cells of the layer V (3 animals) at frequency ranging between 0.03 to 0.33 Hz. At PND19-21, RGNA were recorded in 15/19 cells of the layer II/III (3 animals) and with an higher frequency (ranging between 0.1 to 0.6 Hz) but only in 4/14 cells of the

layer V (3 animals) at frequency ranging between 0.02 to 0.3 Hz. RGNA were no more observed in upper and deep layers in animal aged 4-5 weeks (layer II/III, n = 14 cells, 2 animals; layer V, n= 13 cells, 2 animals).

The mutation had strong consequences on RGNA particularly in the layer II/III. In this layer, at PND 7-9, the occurrence of RGNA as well as the charge transfer produced by these activity in mutant pyramidal cells were significantly increased compared to RGNA recorded in wild type pyramidal cells (n = 19 cells, 4 animals, figure 9A). A significant increase in RGNA frequency was also observed in mutant pyramidal cells at PND19-21 but not associated with an increase in the charge transfer (n = 19 cells, 4 animals, figure 9B). In addition RGNA was present in 100 % of the mutant cells recorded but in 79% of wild type cells. However in spite of the increase in the occurrence of RGNA, total frequency of GABAR-PSC (events in and out RGNA) was not significantly altered suggesting that in the knock-in mice most of postsynaptic events are concentrated in the RGNA. No change in GABAR-PSC frequency was observed at PND28-35, when there was no more RGNA (n = 14 cells, 2 animals, figure 9C). Like for GABAR-PSC, there was no significant difference in the frequency of GluR-PSC between PND7 to PND 35 (figure 9).

Network activity recorded in the layer V showed some differences compared with the layer II/III. The occurrence of RGNA in wild type cell of the layer V and the number of cells in which they have been recorded were less important than in the layer II/ III. This was particularly obvious at PND19-21 where in the layer V, RGNA were observed in ~ 30% of cells while in the layer II/III there we observed in ~80% of cells (figure 10B). Moreover the frequency of RGNA in layer V was on average twice lower than in layer II/III. At PND 7-9 there were ~20% less cells with RGNA in the layer V than in layer II/III (figure 10A). Network activity in the layer V appeared also to be less sensitive to the variant than the layer II/III. Thus in the layer V, at both PND7-9 and PND 19-21, there were no significant differences in the frequency of RGNA and in the charge transfer between wild-type cells and mutant cells (figure 10A,B). However, at PND19-21, RGNA was observed in much more mutant cells than in wild type cells (figure 10B). Finally, like for pyramidal cells of the layer II/III, there were no significant differences in GABAR-PSC and GluR-PSC frequencies in wild-type cells and mutant cells of the layer V at the 3 developmental periods studied (figure 10A-C).

Together these data suggested that the GABAergic network interneurons contributing to RNGA are highly sensitive to the variant, particularly in the layer II/III. Like for the electrophysiological properties of pyramidal cells this sensitivity appears also developmentally regulated.

Discussion

The physiopathological mechanisms of EOEE are actually unknown even if variants in several genes and in particular in *KCNQ2* have been identified (Weckyusen et al., 2012; Kato et al., 2013; Milh et al., 2013; McTague et al., 2016; Allen et al., 2020; see also http://www.rikee.org). Preliminary electrophysiological studies performed in non-neuronal cells have shown that variants have clear functional consequences on M current, loss of function effects being the most common mechanism, although gain of function of M current has also been reported (Miceli et al., 2015; Devaux et al., 2016) as well as change in subcellular channel distribution (Abidi et al., 2015).

The generation of a knock-in mouse model carrying the heterozygous c.821C>T variant in the *KCNQ2* gene (p.T274M for the protein) identified in several patients, offers the opportunity to study the consequences of a loss of function variant both *in vivo* and *ex-vivo* at cellular and network levels to better understand how a pathogenic variant affects brain development and in future test pharmacological compounds that could be used to improve neurological function (Milh et al.,2020). However at a first step it was essential to demonstrate that the variant had clearly functional consequences and that this model presents some reminiscence with EOEE. A recent study performed in this animal model aged 5 weeks reported important cognitive deficits and spontaneous lethal seizures in ~20% of animals suggesting that the variant had clearly pathological consequences (Milh et al., 2020). Moreover, the p.T274M variant has also been show to slow locomotor rhythm-generating network in an in vitro spinal cord preparation from neonatal rats (Verneuil et al., 2020). Here, we clearly show that the heterozygous p.T274M variant increases the excitability of cortical pyramidal cells and affects synapse-driven network activity, however with some differences depending on the location of cells in cortical layers and during a restricted period of development.

Thus, we observed that in the layer II/III, there was a strong parallelism between the effect of the variant and of the M channel blocker XE-991 on the intrinsic properties of pyramidal cells until PND19-21. The responses of the cells to the injection of steps or ramp of current were similarly impacted by the variant or the blocker with a general increase in neuronal excitability up to a certain level of current injected. These results obtained are in keeping to what is expected of the role of Kv7 channels in the control of neuronal excitability and in particular the fact that they play fundamental role to limit the neuronal firing and reduce the frequency of discharge. Moreover, the ramp protocol which should revealed much better the role of these channels on neuronal response than current steps showed that both mutant and XE-991 treated wild type cells discharged at higher frequency and for lower amount of current injected than wild type cells. These results support also the notion that the electrophysiological consequences of the variant on cellular properties is related to a decrease in M current efficiency and a concomitant increase in the resistance of cells at potentials where M current are normally activated. These data also suggest that Kv7.2 subunit may strongly contribute to M

current in layer II/III. This is in keeping with a recent study, although performed in the somatosensory cortex, showing that the conditional ablation of *KCNQ2* or the transfection by electroporation of the pathogenic p.I205V variant –related to EOEE leads to an hyperexcitability of pyramidal cells of the layer II/III (Niday et al. 2017). Our data also indicated that Kv7 channels control neuronal excitability of pyramidal cells of the layer II/III of the motor cortex already during the neonatal period. The presence of M current was also detected in acute dissociated pyramidal cells of the layer II/III of somatosensory cortex, CA1 and CA3 pyramidal cells of the hippocampus, lumbar interneurons of the spinal chord from rodents aged one week (Safuilina et al., 2008; Guan et al., 2011; Marguet et al., 2015; Verneuil et al., 2020). This indicates that early functional expression of these channels is a common feature of several regions and even if there are expressed to a much lower level than at juvenile and adult stages they seem play fundamental role for proper brain development (Peters et al., 2005; Marguet et al. 2017).

A different situation seems to prevail for pyramidal cells of the layer V. We observed two major differences with pyramidal cells of the layer II/III. First, these cells were insensitive to the variant and to XE-991 at PND7-9 and second, at PND19-21, their responses to the injection of steps or to a ramp of current were much more sensitive to XE-991 than to the variant. There are several possible interpretations for these results. At PND 7-9, i) Kv7 channels are not produced or not expressed at the membrane of pyramidal cells. However, very preliminary western blot experiments showed that Kv7.2, 3 and 5 subunits are produced in the layer V (data not shown); ii) Kv7 channels are expressed but only composed by homomeric Kv7.5 subunits or by heteromeric association of Kv7.3 with Kv7.5 subunit. Indeed, current mediated by these two combinations of subunits is much less sensitive to XE-991 than mediated by channels containing Kv7.2 subunit and would not be or slightly affected by 20 µM of XE-991 used in the present study (Schroeder et al., 2000). If this indeed the explanation this would indicate that Kv7 channels in pyramidal cells of layer II/III and layer V are not composed by same subunits. It is well known that there are differences in the expression of ion channels and intrinsic properties of cells of a same structure. This has been documented in particular in the superficial and deep layers of CA1 and CA3 pyramidal cells, between CA3 and CA1 pyramidal cells or between CA1 pyramidal cells of dorsal and frontal hippocampus (Tzingounis et al., 2010; Mizuseki et al., 2011; Marissal et al., 2012; Hönigsperger et al., 2015). Thus, for example and regarding the composition of Kv7 channels it has been shown that Kv7.2,3,5 subunits coexist in CA3 pyramidal cells but with a high proportion of Kv7.5 subunit which participate to the mAHP and slow AHP in these cells whereas in the CA1 pyramidal cells the expression of Kv7.5 is low and M current is mainly mediated by Kv7.2/Kv7.3 (Tzingounis et al., 2010); iii) the response of the wild-type cells to the injection of steps or to a ramp of current is saturated and cannot be further increased by the blocker or the variant. We noticed that the response of the cells of the layer V to the injection of current steps is stronger than cells of the layer II/III; iv) Kv7 channels are expressed but at PND7-9, they play a

minor role in the control of intrinsic properties of pyramidal cells of the layer V in comparison to the action of other ion channels. Among them, one can cite Ether-a-go-go-Related Gene (ERG) K^+ channels which are highly expressed in neocortical pyramidal cells (Saganich et al., 2001; Papa et al., 2003), contributing to M-like current in mammalian neuronal cell and acting as brake in neuronal firing (Selyanko et al., 1999; Cui and Strowbridge, 2018).

We observed that at PN19-21, XE-991 strongly impacted the excitability of pyramidal cells of the layer V and to a higher level than did by the variant. In addition the response of the cells to the injection of a slow ramp of current showed that the variant affected only and slightly some of the parameters analyzed in contrast to XE-991 which affected more deeply most of the parameters. The sensitivity of pyramidal cells to the variant and to XE-991 in this layer is different to what was observed in the layer II/III. These results are difficult to interpret because at a first glance this could suggest that Kv7.2 or Kv7.2/Kv7.3 are not the main contributor of M current in layer V of motor cortex of the 129Sv mice. However, this is unlikely because as it is mentioned above, M current mediated by homomeric Kv7.5 or heteromeric Kv7.3/Kv7.5 channels displayed low sensitivity to XE-991. Therefore, there are 2 possible explanations at least: either, for an unknown reason, the inhibitory impact of the pT274M variant on Kv7channels is lower in pyramidal cells of the layer V than in the layer II/III or that a mechanism of compensation starts to take place in the layer V (but not in the layer II/III) limiting the effect of the mutant channels. Whatever the reasons, these results show, that until PND 19-21, the variant does not homogeneously impact the properties of the pyramidal cells of the upper and deep layers. This is clearly not the case at PND28-35. Properties of pyramidal cells of the upper and deep layers were unaffected by the variant but still sensitive to XE-991 indicating that some forms of plasticity occurred in these cells allowing the recovery of control excitability. Several studies have demonstrated the plasticity of the AIS in response to chronic alteration of neuronal activity and serving as a homeostatic purpose (Kuba et al., 2010; Grubb and Burrone, 2010; Adachi et al., 2015; Wefelmeyer et al., 2016; Lezmy et al., 2017; Engelhardt et al., 2019). These studies included experiments in which Kv7 channels were chronically blocked in cultured neurons which consequences was an increase in neuronal discharge but for a limited period of time before a full recovery of the control excitability (Lezmy et al., 2017). This recovery was associated with a distal shift of the AIS. Our data show also a significative distal shift of the AIS of both pyramidal cells of the layer II/III and V from knock-in mice aged 4-5 weeks, and without any change in the total length. Although the AIS-soma distance is on average multiplied by 4 in cells from the knock-in mice, this displacement nevertheless remains small and it is difficult to appreciate if this has relevant consequence on neuronal excitability also because somato-dendritic morphology and dendritic arborization may strongly influence neuronal excitability (Gulledge and Bravo, 2016); a parameter that has not yet been analyzed in the present study. In addition, change in the properties /expression of other ion channels could also be impacted at long-term by the variant in both activity dependent and

activity independent manner allowing the restoration of control excitability (Marder and Prinz, 2002; MacLean et al., 2003; Marder and Goaillard, 2006; Turrigiano, 2011). Whatever, our data reveal that some changes occur in the action potential trigger zone of mutant cells that are not observed at earlier developmental stages when variant increased neuronal excitability.

Our data showed that the variant affected not only the intrinsic properties of pyramidal cells but may also probably affect the properties of interneurons. This was suggested from the analysis of spontaneous synaptic activity. We observed the presence of spontaneous network driven events that were mediated by GABA receptors (called RGNA), and more often observed in the layer II/III than in the layer V. We found that RGNA recorded in the layer II/III were highly sensitive to the variant and in particular their frequency and number of cells where they have been recorded which were increased in the knock-in mice. Spontaneous network -driven activities have been described in several developing structures including the hippocampus (Ben-Ari et al., 1989, 2007; Garaschuk et al., 1998), the neocortex (Garaschuk et al., 2000; Allene et al., 2008; Modol et al., 2017) where they were called giant depolarizing potential (GDPs) or early network oscillations (ENOs), the spinal cord (Landmesser and O'Donovan et al., 1984), the retina (Meister et al., 1991). In the cortex these patterns modify the efficacy of developing GABAergic and glutamatergic synapses and are likely to play important role in the wiring of neuronal circuit (Ben-Ari et al., 2007; Griguoli and Cherubini, 2017). Interestingly, in the hippocampus change in the frequency of GDPs (increase or decrease) has been reported in some animal models of neurodevelopmental disorders (Griguoli and Cherubini, 2017). However RGNA display some differences with GDPs/ENOs. Indeed; i) they were still observed in the presence of glutamate receptors antagonists, suggesting they do not necessitate pyramidal cells activation for their generation; ii) they seems largely or exclusively mediated by GABA receptors while GDPs/ENOs contain a glutamatergic component (Khalilov et al., 2015). The absence of contribution of glutamate receptors in RGNA may probably be due to the fact that pyramidal cells did not fire action potential during the burst of GABAR-PSCs even at P7 when GABA exerts its excitatory action (Ben-Ari et al. 2007). Indeed, we observed that pyramidal cells were silent when recorded in cell-attached configuration; iii) RGNA are observed at PND19-21, in particular in the layer II/III and even with an higher frequency than at PND7-9 while GDP/ENOs disappeared in cortical slices from rodents aged one-two weeks. It is possible that the differences in the properties of RGNA and GDPs/ENOs are related to the cortical structure analyzed and/or the rodents used. In the hippocampus synaptic-driven network patterns are orchestrated by a subpopulation of pioneer early born gabaergic interneurons expressing somatostatin, possessing widespread axonal arborization and acting as hub cells (Bonifazzi et al ., 2010; Picardo et al., 2011). Existence of GABAergic hub cells has also been described in the entorhinal cortex and they are likely to exist in other neocortical region such as the motor cortex to orchestrate network activity (Modol et al., 2017). We speculate that Kv7 channels incorporating Kv7.2 subunits play important role in the firing properties of these cells. However the reasons why the

variant impacts RGNA in the layer II/III but much less in the layer V (only the number of cells in which RGNA was observed is increased in this layer at PND19-21) is difficult to understand notably because some interneurons including hub cells of both layers may be interconnected which would allow the propagation of RGNA from one layer to another (Jiang et al., 2015; Modol et al., 2017). There are at present some data regarding the expression and function of Kv7 channels in interneurons. Studies have essentially been performed in hippocampal interneurons where expression and modulation of neuronal firing by Kv7 channels have been demonstrated for regular and fast spiking interneurons maintained in primary hippocampal cultures (Grigorov et al., 2014), in a subset of somatostatin oriens-lacunosum moleculare (OLM) interneurons and paravalbumin expressing interneurons in the CA1 region of the hippocampus; in the basket cells, OLM and bistratified interneurons of the CA3 region of the hippocampus (Lawrence et al., 2006; Nieto-Gonzalez and Jensen 2013; Fidzinski et al., 2015; Soh et al.2018). Recent data provided also evidences for the modulation of neuronal firing by Kv7 channels of paravalbumin expressing interneurons in the layer II/III of the somatosensory cortex (Soh et al., 2018). It is therefore not surprising that Kv7.2 variants affect spontaneous gabaergic activity in the neocortex (the present study) and the hippocampus (Uchida et al, 2017, but see Marguet et al., 2015). Thus an abnormal activity of interneurons should be considered in the pathophysiology of *KCNQ2*-related EOEE.

In summary, in this study we provided evidences that the heterozygous p.T274M variant impacts neuronal excitability and network activity. We highlighted that neurons of the layer II/III are more sensitive to the variant than those located in the layer V, in terms of age of onset, consequences on neuronal firing and spontaneous synaptic driven network activity. Moreover our data suggest the existence of compensatory mechanism in knock-in mice aged 4-5 weeks and occurring at both cellular and network level. These findings are particularly relevant to EOEE knowing that for a majority of patients carrying variants in the *KCNQ2* gene there is a normalization of the electrographic activity and remission of the epilepsy few weeks to several months after seizures onset. In particular the epilepsy of the patient carrying the p.T274M variant was active for only 6 weeks, controlled by anti-epileptic drugs then in remission without treatment from the age of 1 year (Milh et al., 2013). However in spite of this, the patient made almost no motor acquisition, no acquisition of verbal communication. It is tempting to speculate that the normalization of the EEG also results from compensatory mechanisms. Although several questions remain regarding the role of neonatal seizures in patient development, the elucidation of mechanisms of compensation and reasons why this occurs at a particular stage of development represent important aspect of future studies for the understanding of the pathophysiology of EOEE which results may have implication to develop therapies with adapted target.

Acknowledgements: This work was supported by INSERM (Institut National de la Santé et de la Recherche Médicale), by the Agence National pour la Recherche (ANR -19-CE17-0018-02, IMprove), by the Ministère de l'Enseignement Supérieur, de la Recherche et de l'Innovation. We would like to thank Aurélie Montheil and Francesca Bader for mice genotyping (PBMC at INMED) and Dr.François Michel (Imagic at INMED) for his precious help in the use of the confocal microscope and Neurolucida.

Author contributions

N.B. performed and analyzed electrophysiological experiments with H.B and L.A. N.B also performed immunohistochemistry experiments with M.K and H.B and analysed the AIS. L.V provided the knock-in mice. L.A designed and supervised the whole project with N.B. and H.B. L.A wrote the manuscript with the help of M.M

Declaration of Interest

The authors declare no competing financial interests.

References

Abidi A, Devaux JJ, Molinari F, et al. 2015. A recurrent KCNQ2 pore mutation causing early onset epileptic encephalopathy has a moderate effect on M current but alters subcellular localization of Kv7 channels. Neurobiol Dis. 80 :80-92

Adachi R, Yamada R, Kuba H. 2015. Plasticity of the axonal trigger zone. Neuroscientist 21: 255-265.

Allen NM, Mannion M, Conroy J, Lynch SA, Shahwan A, Lynch B, King MD. 2014. The variable phenotypes of KCNQ-related epilepsy. Epilepsia. 55:e99–e105.

Allen NM, Weckhuysen S, Gorman K, King MD. 2020. Genetic Potassium Channel-Associated Epilepsies: Clinical Review of the Kv Family. Eur J Paediatr Neurol. 24 : 105-116.

Battefeld A, Tran BT, Gavrilis J, Cooper EC, Kole MHP. 2014. Heteromeric Kv7.2/7.3 Channels Differentially Regulate Action Potential Initiation and Conduction in Neocortical Myelinated Axons. J Neurosci. 34:3719–3732.

Ben-Ari Y, Cherubini E, Corradetti R, Gaiarsa JL.1989. Giant synaptic potentials inimmature rat CA3 hippocampal neurones. J Physiol 416:303-25.

Ben-Ari Y, Gaiarsa JL, Tyzio R, Khazipov R. 2007. GABA: A pioneer transmitter that excites immature neurons and generates primitive oscillations. Physiol Rev. 87:1215–1284.

Bonifazi P, Goldin M, Picardo MA, Jorquera I, Cattani A, Bianconi G, Represa A, Ben-Ari Y, Cossart R. 2009. GABAergic hub neurons orchestrate synchrony in developing hippocampal networks. Science. 326:1419–1424.

Brown DA, Passmore GM. 2009. Neural KCNQ (Kv7) channels. Br J Pharmacol. 156:1185–1195.

Cui ED, Strowbridge BW. 2018. Modulation of Ether-à-Go-Go Related Gene (ERG) Current Governs Intrinsic Persistent Activity in Rodent Neocortical Pyramidal Cells. J Neurosci. 38:423–440.

Delmas P, Brown DA. 2005. Pathways modulating neural KCNQ/M (Kv7) potassium channels. Nat Rev Neurosci. 6:850–862.

Desai NS, Rutherford LC, Turrigiano GG. 1999. Plasticity in the intrinsic excitability of cortical pyramidal neurons. Nat Neurosci. 2:515–520.

Devaux JJ, Kleopa KA, Cooper EC, Scherer SS. 2004. KCNQ2 Is a Nodal K+ Channel. J Neurosci. 24:1236–1244.

Engelhardt M, Jamann N, Wefelmeyer W. 2019. Small domain, large consequences: The axon initial segment as a key player in neuronal excitability. Neuroforum. 25:49–60.

Fidzinski P, Korotkova T, Heidenreich M, Maier N, Schuetze S, Kobler O, Zuschratter W, Schmitz D, Ponomarenko A, Jentsch TJ. 2015. KCNQ5 K+ channels control hippocampal synaptic inhibition and fast network oscillations. Nat Commun. 6:1–13.

Garaschuk O, Hanse E, Konnerth A. 1998. Developmental profile and synaptic origin of early network oscillations in the CA1 region of rat neonatal hippocampus. J Physiol. 507:219–236.

Garaschuk O, Linn J, Eilers J, Konnerth A.2000. Large-scale oscillatory calcium waves in the immature cortex. Nat Neurosci 3:452-9.

Greene DL, Hoshi N. 2017. Modulation of Kv7 channels and excitability in the brain. Cell Mol Life Sci. 74:495–508.

Grubb MS, Burrone J. 2010. Activity-dependent relocation of the axon initial segment fine-tunes neuronal excitability. Nature. 465:1070–1074.

Gu N, Vervaeke K, Hu H, Storm JF. 2005. Kv7/KCNQ/M and HCN/h, but not KCa2/SK channels, contribute to the somatic medium after-hyperpolarization and excitability control in CA1 hippocampal pyramidal cells. J Physiol. 566:689–715.

Guan D, Higgs MH, Horton LR, Spain WJ, Foehring RC. 2011. Contributions of Kv7-mediated potassium current to sub- and suprathreshold responses of rat layer II/III neocortical pyramidal neurons. J Neurophysiol. 106:1722–1733.

Gulledge AT, Bravo JJ. 2016. Neuron Morphology Influences Axon Initial Segment plasticity. Eneuro. 3:1–24.

Grigorov A, Moskalyuk A, Kravchenko M, Veselovsky N, Verkhratsky A, Fedulova S. 2014. Kv7 potassium channel subunits and M currents in cultured hippocampal interneurons. Pflugers Arch Eur J Physiol. 466:1747–1758.

Griguoli M, Cherubini E. 2017. Early correlated network activity in the hippocampus: Its putative role in shaping neuronal circuits. Front Cell Neurosci. 11:1–11.

Hu H, Vervaeke K, Storm JF. 2002. Two forms of electrical resonance at theta frequencies, generated by M-current, h-current and persistent Na+ current in rat hippocampal pyramidal cells. J Physiol. 545:783–805.

Hu H, Vervaeke K, Storm JF. 2007. M-Channels (Kv7/KCNQ Channels) That Regulate Synaptic Integration, Excitability, and Spike Pattern of CA1 Pyramidal Cells Are Located in the Perisomatic Region. J Neurosci. 27:1853–1867.

Hu W, Bean BP. 2018. Differential Control of Axonal and Somatic Resting Potential by Voltage-Dependent Conductances in Cortical Layer 5 Pyramidal Neurons. Neuron. 97:1315-1326.

Huang H, Trussell LO. 2011. KCNQ5 channels control resting properties and release probability of a synapse. Nat Neurosci. 14:840–847.

Jentsch TJ. 2000. Neuronal KCNQ potassium channels: Physiology and role in disease. Nat Rev Neurosci. 1:21–30.

Hönigsperger C, Marosi M, Murphy R, Storm JF. 2015. Dorsoventral differences in Kv7/M-current and its impact on resonance, temporal summation and excitability in rat hippocampal pyramidal cells. J Physiol. 593:1551–1580.

Jiang X, Shen S, Cadwell CR, Berens P, Sinz F, Ecker AS, Patel S, Tolias AS. 2015. Principles of connectivity among morphologically defined cell types in adult neocortex. Science 350. aac 9462

Kato M, Yamagata T, Kubota M, et al. 2013. Clinical spectrum of early onset epileptic encephalopathies caused by KCNQ2 mutation. Epilepsia. 54:1282–1287.

Khalilov I, Minlebaev M, Mukhtarov M, Khazipov R. 2015. Dynamic changes from depolarizing to hyperpolarizing GABAergic actions during giant depolarizing potentials in the neonatal rat hippocampus. J Neurosci. 35:12635–12642.

Kuba H, Oichi Y, Ohmori H. 2010. Presynaptic activity regulates Na^+ channel distribution at the axon initial segment. Nature. 465:1075–1078.

Landmesser LT, O'Donovan MJ.1984. Activation patterns of embryonic chick hind limb muscles recorded in ovo and in an isolated spinal cord preparation. J Physiol 347:189-204.

Lawrence JJ, Saraga F, Churchill JF, Statland JM, Travis KE, Skinner FK, McBain CJ. 2006. Somatodendritic Kv7/KCNQ/M channels control interspike interval in hippocampal interneurons. J Neurosci. 26:12325–12338.

Lezmy J, Lipinsky M, Khrapunsky Y, Patrich E, Shalom L, Peretz A, Fleidervish IA, Attali B. 2017. M-current inhibition rapidly induces a unique CK2-dependent plasticity of the axon initial segment. Proc Natl Acad Sci. 114:E10234-E10243.

MacLean JN, Zhang Y, Johnson BR, Harris-Warrick RM. 2003. Activity-independent homeostasis in rhythmically active neurons. Neuron. 37:109–120.

Marder E, Prinz AA. 2002. Modeling stability in neuron and network function: The role of activity in homeostasis. BioEssays. 24:1145–1154.

Marder E, Goaillard JM. 2006. Variability, compensation and homeostasis in neuron and network function. Nat Rev Neurosci. 7:563–574.

Marguet SL, Le-Schulte VTQ, Merseburg A, Neu A, Eichler R, Jakovcevski I, Ivanov A, Hanganu-Opatz IL, Bernard C, Morellini F, Isbrandt D. 2015. Treatment during a vulnerable developmental period rescues a genetic epilepsy. Nat Med. 21:1436–1444.

Marissal T, Bonifazi P, Picardo MA, Nardou R, Petit LF, Baude A, Fishell GJ, Ben-Ari Y, Cossart R. 2012. Pioneer glutamatergic cells develop into a morpho-functionally distinct population in the juvenile CA3 hippocampus. Nat Commun 3:1316.

Martinello K, Giacalone E, Migliore M, Brown DA, Shah MM. 2019. The subthreshold-active KV7 current regulates neurotransmission by limiting spike-induced Ca^{2+} influx in hippocampal mossy fiber synaptic terminals. Commun Biol. 2.145

McTague A, Howell KB, Cross JH, Kurian MA, Scheffer IE. 2016. The genetic landscape of the epileptic encephalopathies of infancy and childhood. Lancet Neurol. 15:304–316.

Meister M, Wong RO, Baylor DA, Shatz CJ. 1991. Synchronous bursts of action potentials in ganglion cells of the developing mammalian retina. Science 252:939-43.

Miceli F, Soldovieri M V., Ambrosino P, Barrese V, Migliore M, Cilio MR, Taglialatela M. 2013. Genotype-phenotype correlations in neonatal epilepsies caused by mutations in the voltage sensor of Kv7.2 potassium channel subunits. Proc Natl Acad Sci. 110:4386–4391.

Milh M, Boutry-Kryza N, Sutera-Sardo J et al. 2013. Similar early characteristics but variable neurological outcome of patients with a de novo mutation of KCNQ2. Orphanet J Rare Dis. 8:0–7.

Milh M, Roubertoux P, Biba N, Chavany J, Spiga Ghata A, Fulachier C, Collins SC, Wagner C, Roux JC, Yalcin B, Félix MS, Molinari F, Lenck-Santini PP ,Villard L.2020 A knock-in mouse model for KCNQ2-related epileptic encephalopathy displays spontaneous generalized seizures and cognitive impairment. Epilepsia. Doi: 10.1111/epi.16494.

Mizuseki K, Diba K, Pastalkova E, Buzsáki G.2011. Hippocampal CA1 pyramidal cells form functionally distinct sublayers. Nat Neurosc 14:1174-81.

Módol L, Sousa VH, Malvache A, Tressard T, Baude A, Cossart R. 2017. Spatial embryonic origin delineates gabaergic hub neurons driving network dynamics in the developing entorhinal cortex. Cereb Cortex. 27:4649–4661.

Niday Z, Hawkins VE, Soh H, Mulkey DK, Tzingounis A V. 2017. Epilepsy-Associated KCNQ2 Channels Regulate Multiple Intrinsic Properties of Layer 2/3 Pyramidal Neurons. J Neurosci. 37:576–586.

Nieto-Gonzalez JL, Jensen K. 2013. BDNF Depresses Excitability of Parvalbumin-Positive Interneurons through an M-Like Current in Rat Dentate Gyrus. PLoS One. 8. e67318

Ohtahara S, Yamatogi Y.2003. Epileptic encephalopathies in early infancy with suppression-burst. J Clin Neurophysiol. 20:398-407.

Orhan G, Bock M, Schepers D, Ilina EI, Reichel SN, Löffler H, Jezutkovic N, Weckhuysen S, Mandelstam S, Suls A, Danker T, Guenther E, Scheffer IE, De Jonghe P, Lerche H, Maljevic S. 2014. Dominant-negative effects of KCNQ2 mutations are associated with epileptic encephalopathy. Ann Neurol. 75:382–394.

Papa M, Boscia F, Canitano A, Castaldo P, Sellitti S, Annunziato L, Taglialatela M. 2003. Expression pattern of the ether-a-gogo-related (ERG) K+ channel-encoding genes ERG1, ERG2, and ERG3 in the adult rat central nervous system. J Comp Neurol. 466:119–135.

Peters HC, Hu H, Pongs O, Storm JF, Isbrandt D. 2005. Conditional transgenic suppression of M channels in mouse brain reveals functions in neuronal excitability, resonance and behavior. Nat Neurosci. 8:51–60.

Picardo MA, Guigue P, Bonifazi P, Batista-Brito R, Allene C, Ribas A, Fishell G, Baude A, Cossart R. 2011. Pioneer GABA cells comprise a subpopulation of hub neurons in the developing hippocampus. Neuron. 71:695–709.

Safiulina VF, Zacchi P, Taglialatela M, Yaari Y, Cherubini E. 2008. Low expression of Kv7/M channels facilitates intrinsic and network bursting in the developing rat hippocampus. J Physiol. 586:5437–5453.

Saganich MJ, Machado E, Rudy B. 2001. Differential expression of genes encoding subthreshold-operating voltage-gated K+ channels in brain. J Neurosci. 21:4609–4624.

Selyanko AA, Hadley JK, Wood IC, Abogadie FC, Delmas P, Buckley NJ, London B, Brown DA. 1999. Two types of K+ channel subunit, Erg1 and KCNQ2/3, contribute to the M- like current in a mammalian neuronal cell. J Neurosci. 19:7742–7756.

Schroeder BC, Hechenberger M, Weinreich F, Kubisch C, Jentsch TJ. 2000. KCNQ5, a Novel Potassium Channel Broadly Expressed in Brain, Mediates M-type Currents. J Biol Chem. 275:24089–24095.

Shah MM, Migliore M, Valencia I, Cooper EC, Brown DA. 2008. Functional significance of axonal Kv7 channels in hippocampal pyramidal neurons. Proc Natl Acad Sci U S A. 105:7869–7874.

Shah MM, Migliore M, Brown DA. 2011. Differential effects of Kv7 (M-) channels on synaptic integration in distinct subcellular compartments of rat hippocampal pyramidal neurons. J Physiol. 589:6029–6038.

Simkin D, Searl TJ, Piyevsky BN, et al. 2019. Impaired M-current in KCNQ2 Encephalopathy Evokes Dyshomeostatic Modulation of Excitability.
bioRxiv 538371; doi: https://doi.org/10.1101/538371

Soh H, Pant R, LoTurco JJ, Tzingounis A V. 2014. Conditional Deletions of Epilepsy-Associated KCNQ2 and KCNQ3 Channels from Cerebral Cortex Cause Differential Effects on Neuronal Excitability. J Neurosci. 34:5311–5321.

Soh H, Park S, Ryan K, Springer K, Maheshwari A, Tzingounis A V. 2018. Deletion of KCNQ2/3 potassium channels from PV+ interneurons leads to homeostatic potentiation of excitatory transmission. Elife. 1–14.

Storm JF. 1990. Potassium currents in hippocampal pyramidal cells. Prog Brain Res. 83:161–187.

Turrigiano G. 2011. Too Many Cooks? Intrinsic and Synaptic Homeostatic Mechanisms in Cortical Circuit Refinement. Annu Rev Neurosci. 34:89–103.

Tzingounis A V., Heidenreich M, Kharkovets T, Spitzmaul G, Jensen HS, Nicoll RA, Jentsch TJ. 2010. The KCNQ5 potassium channel mediates a component of the afterhyperpolarization current in mouse hippocampus. Proc Natl Acad Sci U S A. 107:10232–10237.

Uchida T, Lossin C, Ihara Y, Deshimaru M, Yanagawa Y, Koyama S, Hirose S. 2017. Abnormal γ-aminobutyric acid neurotransmission in a Kcnq2 model of early onset epilepsy. Epilepsia. 58:1430–1439.

Vervaeke K, Gu N, Agdestein C, Hu H, Storm JF. 2006. Kv7/KCNQ/M-channels in rat glutamatergic hippocampal axons and their role in regulation of excitability and transmitter release. J Physiol. 576:235–256.

Verneuil J, Brocard C, Villard L, Peyronnet-Roux J. Bocard F. 2020. It takes two to tango : M-current swings with the persistent sodium current to set the speed of locomotion.
biorxiv.org/content/10.1101/2020.04.24.059311v1

Wang HS, Pan Z, Shi W, Brown BS, Wymore RS, Cohen IS, Dixon JE, McKinnon D. 1998. KCNQ2 and KCNQ3 potassium channel subunits: Molecular correlates of the M-channel. Science 282:1890–1893.

Weckhuysen S, Mandelstam S, Suls A, et al. 2012. KCNQ2 encephalopathy: Emerging phenotype of a neonatal epileptic encephalopathy. Ann Neurol. 71:15–25.

Wefelmeyer W, Puhl CJ, Burrone J. 2016. Homeostatic Plasticity of Subcellular Neuronal Structures: From Inputs to Outputs. Trends Neurosci. 39:656–667.

Yue C, Yaari Y. 2006. Axo-somatic and apical dendritic Kv7/M channels differentially regulate the intrinsic excitability of adult rat CA1 pyramidal cells. J Neurophysiol. 95:3480–3495.

Layer II/III	**PND 7-9** ***KCNQ2$^{WT/WT}$*** (n = 16 cells, 2 mice) ***KCNQ2$^{WT/WT}$* in XE-991** (n = 11 cells, 2 mice) ***KCNQ2$^{WT/p.T274M}$*** (n = 15 cells, 3 mice)	**PND 19-21** ***KCNQ2$^{WT/WT}$*** (n = 14 cells, 3 mice) ***KCNQ2$^{WT/WT}$* in XE-991** (n = 15 cells, 3 mice) ***KCNQ2$^{WT/p.T274M}$*** (n = 15 cells, 3 mice)	**PND 28-35** ***KCNQ2$^{WT/WT}$*** (n = 19 cells, 4 mice) ***KCNQ2$^{WT/WT}$* in XE-991** (n = 18 cells, 4 mice) ***KCNQ2$^{WT/p.T274M}$*** (n = 19 cells, 3 mice)
Cm (pF)	58.3 ± 6.1 59.0 ± 4.1 57.0 ± 3.7	108.5 ± 7.0 113.3 ± 7.1 122.7 ± 9.9	131.6 ± 12.4 112.9 ± 6.8 110.1 ± 12.3
Vrest (mV)	-66.2 ± 0.8 -67.8 ± 2.1 -65.9 ± 1.5	-69.6 ± 1.2 -67.3 ± 1.4 -71.7 ± 1.3	-74.8 ± 1.3 -68.8 ± 1.6§§§ -74.1 ± 0.6
Rm (mOhm)	312.6 ± 22.8 483.5 ± 33.1§§§ 590.9 ± 55.8 ***	168.1 ± 15.8 199.7 ± 14.5 176.3 ± 22.6	152.1 ± 18.5 207.9 ± 15.7§ 187.5 ± 23.7
τ_m (msec)	24.9 ± 1.7 26.7 ± 3.2 27.3 ± 2.6	17.3 ± 1.3 20.3 ± 1.6 19.3 ± 1.1	15.5 ± 0.9 20.4 ± 2.3 17.4 ± 1.4
Action potential properties			
I threshold (pA)	327.5 ± 14.1 218.2 ± 8.7 §§§ 210.7 ± 15.2***	417.9 ± 40.1 464.3 ± 22.5 466.7 ± 39.1	502.6 ± 40.9 367.6 ± 33.8* 411.1 ± 38.9
Vm threshold (mV)	-37.9 ± 0.8 ; -43.2 ± 0.8§§§ -40.5 ± 0.6*	-37.7 ± 1.2 -45.9 ± 1.1§§§ -40.5 ± 1.7	-44.0 ± 0.8 -46.1 ± 0.9 -43.6 ± 0.7
Amplitude (mV)	71.9 ± 1.4 76.1 ± 1.3 71.8 ± 2.0	81.5 ± 2.2 81.1 ± 1.8 83.9 ± 2.8	93.5 ± 1.2 94.8 ± 2.0 87.7 ± 2.1
Overshoot (mV)	35.9 ± 1.2 34.9 ± 1.4 33.1 ± 1.6	45.6 ± 1.4 46.2 ± 1.3 45.2 ± 1.8	49.3 ± 0.9 49.0 ± 1.6 43.9 ± 1.8
Halfwidth (msec)	1.1 ± 0.08 1.3 ± 0.12 0.9 ± 0.03	0.66 ± 0.03 0.82 ± 0.04§§ 0.79 ± 0.05*	0.75 ± 0.03 0.91 ± 0.07 0.76 ± 0.04

Table 1: Intrinsic properties of pyramidal cells of the layer II/III in motor cortical slices from *KCNQ2$^{WT/WT}$* mice (black), in slices from *KCNQ2$^{WT/WT}$* mice superfused with XE-991 (20 µM, green), in slices from *KCNQ2$^{WT/T274M}$* mice (blue) aged one week, three weeks and 4-5 weeks. Number of cells and animals used in each conditions are indicated in parenthesis. Statistics: * *KCNQ2$^{WT/T274M}$* (mutant cells) vs *KCNQ2$^{WT/WT}$* (wild type cells) ; § *KCNQ2$^{WT/WT}$ in XE-991* (XE-991 treated wild type cells) vs *KCNQ2$^{WT/WT}$* (wild type cells). *§ : p< 0.05 ; **,§§ : p< 0.01 ; ***,§§§ p<0.001.

Layer V	**PND 7-9** ***KCNQ2$^{WT/WT}$*** (n = 15 cells, 3 mice) ***KCNQ2$^{WT/WT}$ in XE-991*** (n = 11 cells, 3 mice) ***KCNQ2$^{WT/p.T274M}$*** (n = 15 cells, 3 mice)	**PND 19-21** ***KCNQ2$^{WT/WT}$*** (n = 14 cells, 4 mice) ***KCNQ2$^{WT/WT}$ in XE-991*** (n = 14 cells, 3 mice) ***KCNQ2$^{WT/p.T274M}$*** (n = 15 cells, 4 mice)	**PND 28-35** ***KCNQ2$^{WT/WT}$*** (n = 16 cells, 4 mice) ***KCNQ2$^{WT/WT}$* in XE-991** (n = 14 cells, 3 mice) ***KCNQ2$^{WT/p.T274M}$*** (n = 15 cells, 3 mice)
Cm (pF)	52.7 ± 6.8 59.2 ± 4.5 58.6 ± 8.4	115.5 ± 8.4 107.3 ± 14.4 123.9 ± 11.6	118.9 ± 11.5 99.9 ± 11.9 98.8 ± 8.9
Vrest (mV)	-63.5 ± 1.5 -63.3 ± 1.3 -62.2 ± 2.0	-69.4 ± 1.4 -67.4 ± 2.1 -70.6 ± 0.9	-67.3 ± 1.7 -68.9 ± 1.9 -68.7 ± 1.3
Rm (mOhm)	538.6 ± 59.4 485.5 ± 60.9 427.3 ± 63.8	150.1 ± 24.5 296.4 ± 38.6§§ 142.0 ± 13.3	179.2 ± 13.3 239.6 ± 33.9 180.8 ± 21.4
τ_m (msec)	23.5 ± 2.1 22.7 ± 2.3 24.7 ± 2.5	17.2 ± 2.8 22.9 ± 2.0 18.9 ± 1.6	19.4 ± 1.6 20.2 ± 2.9 16.8 ± 1.2
Action potential Properties			
I threshold (pA)	233.3 ± 21.4 261.8 ± 20.6 233.3 ± 22.3	478.6 ± 39.1 366.7 ± 30.3§ 542.9 ± 33.9	500 ± 33.5 394.6 ± 34.5§§ 453.3 ± 40.1
Vm threshold (mV)	-37.9 ± 1.1 -39.4 ± 1.5 -37.9 ± 1.1	-45.4 ± 1.0 -46.9 ± 1.2 -44.2 ± 1.2	-44.2 ± 1.4 -45.3 ± 1.3 -45.0 ± 0.9
Amplitude(mV)	75.9 ± 2.5 73.7 ± 2.1 80.6 ± 1.5	89.1 ± 1.5 90.4 ± 2.1 89.8 ± 2.0	88.3 ± 1.5 91.1 ± 1.6 89.3 ± 1.6
Overshoot (mV)	37.9 ± 1.2 36.3 ± 2.6 43.1 ± 2.5	45.9 ± 1.2 45.3 ± 1.3 47.6 ± 2.3	48.0 ± 1.6 50.0 ± 1.4 45.8 ± 1.2
Halfwidth (msec)	1.2 ± 0.1 1.4 ± 0.1 1.0 ± 0.07	0.61 ± 0.02 0.85 ± 0.03§§§ 0.76 ± 0.04**	0.84 ± 0.04 0.81 ± 0.02 0.82 ± 0.04

Table 2: Intrinsic properties of pyramidal cells of the layer V in motor cortical slices from *KCNQ2$^{WT/WT}$* mice (black), in slices from *KCNQ2$^{WT/WT}$* mice superfused with XE-991 (20 µM, green), and in slices from *KCNQ2$^{WT/T274M}$* mice (red) aged one week, three weeks and 4-5 weeks. Number of cells and animals used are indicated in parenthesis. Statistics: * *KCNQ2$^{WT/T274M}$* (mutant cells) vs *KCNQ2$^{WT/WT}$* (wild type cells) ; § *KCNQ2$^{WT/WT}$ in XE-991* (XE-991 treated wild type cells) vs *KCNQ2$^{WT/WT}$* (wild type cells). *§ : p< 0.05 ; **,§§ : p< 0.01 ; ***,§§§ p<0.001.

Figure Legends

Figure 1 : Mice genotyping polymerase chain reaction (PCR) using mouse genomic DNA as a template and primers 284-Oht and 281-Oht (the protocol used for PCR is described in the material and method). (T-). PCR without DNA served as a negative control.(T+/+) migration of an animal WT observation of 1 band at 603 bp.(T+/-) migration of a heterozygous animal for the T274M variant, observation of 1 band at 603 bp and 2 bands at 688 bp. MWM, molecular weight marker.The results are shown for 5 animals from the same litter (1 to 5). Animals 1,2,4,5 are WT and animal 3 is a heterozygous animal for the T274M variant.

Figure 2: Effects of XE-991 and of the p.T274M variant on the discharge of developing pyramidal cells of the layer II/III elicited by the injection of steps of current.

Aa) Representative traces showing the recordings of pyramidal cells of the layer II/III in cell-attached configuration in motor cortical slices from a $KCNQ2^{WT/WT}$ mouse (left traces, black), from a $KCNQ2^{WT/WT}$ mouse and superfused with 20 µM XE-991 (middle traces, green) , from a $KCNQ2^{WT/T274M}$ mouse (left trace, blue) and aged one week (Post-Natal Days 7-9). **Ab)** Same cells recorded in whole cell configuration and showing the voltage responses to the injection of three depolarizing current steps of 20, 100 and 220 pA applied during 1 sec. **Ac)** Graphs showing the quantification (mean ± S.E.M) at PND7-9 of the number of action potentials elicited by the injection of depolarizing current steps (left graph), the initial frequency (measured during the first 200 msec of the steps, middle graph) and final frequency (measured during the last 200 msec of the steps, right graph) of the discharge. Black: wild-type cells (n = 16 cells, 2 animals); green: XE-991 treated wild type cells (n = 11 cells, 2 animals); blue: mutant cells (n = 15, 3 animals). **B)** Same quantification as in Ac in cells from mice aged three weeks (PND 19-21). Black: wild-type cells (n = 14 cells, 3 animals); green: XE-991 treated wild type cells (n = 15 cells, 3 animals); blue: mutant cells (n = 15 cells, 3 animals). **C)** Same quantification of the three parameters in cells from mice aged four-five weeks (PND 28-35). Black: wild type cells (n = 19 cells, 4 animals); green: XE-991 treated wild type cells (n = 18 cells, 4 animals); blue: mutant cells (n = 18 cells, 3 animals). Statistics: * $KCNQ2^{WT/T274M}$ (mutant cells) vs $KCNQ2^{WT/WT}$ (wild type cells) ; § $KCNQ2^{WT/WT}$ in XE-991 (XE-991 treated wild type cells) vs $KCNQ2^{WT/WT}$ (wild type cells). *§ : $p< 0.05$; **,§§ : $p< 0.01$; ***,§§§ $p<0.001$.

Figure 3: Effects of XE-991 and of the p.T274M variant on the voltage responses of developing pyramidal cells of the layer II/III to the injection of a ramp of current.

A) Traces showing the response of pyramidal cells to the injection of a ramp of 300 pA in 10 sec recorded in motor cortical slices from $KCNQ2^{WT/WT}$ (black), $KCNQ2^{WT/WT}$ in presence of XE-991 (green) and $KCNQ2^{WT/T274}$ (blue) mice aged one week. Below traces: Histograms representing the quantification (mean ± S.E.M) in the three group of cells of the chord resistance, the current and

voltage threshold of first action potential generation, the number of action potential, the initial frequency (first 1sec of the discharge). Black: wild type cells (n = 16 cells, 2 animals); green: XE-991 treated wild type cells (n = 11 cells, 2 animals); blue: mutant cells (n = 15 cells, 3 animals). **B)** Same as in A in cells from mice aged three weeks. Analysis were performed on the voltage response elicited by the injection of a ramp of 500 pA in 10 sec. Black: wild-type cells (n = 14 cells, 3 animals); green: XE-991 treated wild type cells (n = 15 cells, 3 animals); blue: mutant cells (n = 15 cells, 3 animals). **C)** Same as in B in cells from mice aged 4-5 weeks. Black: wild type cells (n = 19 cells, 4 animals); green: XE-991 treated wild type cells (n = 18 cells, 4 animals); blue: mutant cells (n = 18 cells, 3 animals). Statistics: * $KCNQ2^{WT/T274M}$ (mutant cells) vs $KCNQ2^{WT/WT}$ (wild type cells) ; § $KCNQ2^{WT/WT}$ in XE-991 (XE-991 treated wild type cells) vs $KCNQ2^{WT/WT}$ (wild type cells). *§ : p< 0.05 ; **,§§ : p< 0.01 ; ***,§§§ p<0.001.

Figure 4. Effects of XE-991 and of the p.T274M variant on the discharge of developing pyramidal cells of the layer V elicited by the injection of steps of current.

A) Left column: Representative traces showing the voltage responses to the injection of 100 pA for 1 sec in pyramidal cells of the layer V in motor cortical slices from $KCNQ2^{WT/WT}$ (black), $KCNQ2^{WT/WT}$ in presence of XE-991 (green), $KCNQ2^{WT/T274M}$ (red) and aged one week (PND 7-9). Middle column: same as above but in slices from mice aged 3 weeks (PND 19-21) and with an injected current step of 350 pA. Right column: same but in slices from mice aged 4-5 weeks. **B)** Graphs showing the quantification (mean ± S.E.M) of the number of action potentials (left graph) elicited by the injection of depolarizing current steps, the initial and final frequencies of the discharge (middle and right graph respectively) in pyramidal cells from animals aged one week (PND 7-9). Black: wild-type cells (n = 15 cells, 3 animals); green: XE-991 treated wild type cells (n = 11 cells, 3 animals); red: mutant cells (n = 15, 3 animals). **C)** Same quantification in cells from mice aged three weeks (PND 19-21). Black: wild-type cells (n = 14 cells, 4 animals); green: XE-991 treated wild type cells (n = 14 cells, 3 animals); red: mutant cells (n = 15 cells, 4 animals). **D)** Quantification of the three parameters in cells from mice aged four-five weeks (PND 28-35). Black: wild type cells (n = 16 cells, 4 animals); green: XE-991 treated wild type cells (n = 14 cells, 3 animals); red: mutant cells (n = 15 cells, 3 animals). Statistics: * $KCNQ2^{WT/T274M}$ (mutant cells) vs $KCNQ2^{WT/WT}$ (wild type cells) ; § $KCNQ2^{WT/WT}$ in XE-991 (XE-991 treated wild type cells) vs $KCNQ2^{WT/WT}$ (wild type cells). *§ : p< 0.05 ; **,§§ : p< 0.01 ; ***,§§§ p<0.001.

Figure 5: Effects of XE-991 and of the p.T274M variant on the voltage responses of developing pyramidal cells of the layer V to the injection of a ramp of current.

A) Traces showing the response of pyramidal cells to the injection of a ramp of 300 pA in 10 sec recorded in motor cortical slices from $KCNQ2^{WT/WT}$ (black), $KCNQ2^{WT/WT}$ in presence of XE-991

(green) and *KCNQ2*$^{WT/T274}$ (blue) mice aged one week. Below traces: Histograms representing the quantification (mean ± S.E.M) in the three group of cells of the chord resistance, the current and voltage threshold of first action potential generation, the number of action potential, the initial frequency (first 1sec of the discharge). Black: wild type cells (n = 15 cells, 3 animals); green: XE-991 treated wild type cells (n = 11 cells, 3 animals); red: mutant cells (n = 15 cells, 3 animals). **B)** Same as in A in cells from mice aged three weeks. Analysis were performed on the voltage response elicited by the injection of a ramp of 500 pA in 10 sec. Black: wild-type cells (n = 14 cells, 4 animals); green: XE-991 treated wild type cells (n = 14 cells, 3 animals); red: mutant cells (n = 15 cells, 4 animals). **C)** Same as in B in cells from mice aged 4-5 weeks. Black: wild type cells (n = 16 cells, 4 animals); green: XE-991 treated wild type cells (n = 14 cells, 3 animals); red: mutant cells (n = 15 cells, 3 animals). Statistics: * KCNQ2$^{WT/T274M}$ (mutant cells) vs KCNQ2$^{WT/WT}$ (wild type cells) ; § KCNQ2$^{WT/WT}$ in XE-991 (XE-991 treated wild type cells) vs KCNQ2$^{WT/WT}$ (wild type cells). *§ : p< 0.05 ; **,§§ : p< 0.01 ; ***,§§§ p<0.001.

Figure 6: Measurement of the length of the Axon initial segment (AIS) and of the AIS-soma distance in pyramidal cells of layer the II/III in motor cortical slices from developing *KCNQ2*$^{WT/WT}$ and *KCNQ2*$^{WT/T274M}$ mice.

A) Confocal image of layer II/III of a motor cortical slice from *KCNQ2*$^{WT/WT}$ (right) and from *KCNQ2*$^{WT/T274M}$ (left) mice aged 5 weeks double labeled for NeuN (green) and Ankyrin G (red). Selected cells in rectangle are shown below at an enlarged scale. Note that in wild type mice, AIS are in close contact with cell bodies while the distance AIS-soma is increased in cells from the knock-in mouse (the start of the AIS are indicated by arrows). Scale bar upper images: 50 µm, scale bar lower images: 20 µm. Graphs below show the quantification of the AIS length (left) and of the AIS-soma distance (right) in individual cells from *KCNQ2*$^{WT/WT}$ mice (black dots, n = 99 cells, 3 animals) and *KCNQ2*$^{WT/T274M}$ mice (blue squares, n= 88 cells, 3 animals) aged 5 weeks. Larger symbols are the mean (± S.E.M) of the values from the 2 groups of mice. **B**) Same quantification in cells from mice aged one week. *KCNQ2*$^{WT/WT}$ (n = 85 cells, 3 animals), *KCNQ2*$^{WT/T274M}$ (n= 60 cells, 3 animals); **C)** Quantification in cells from mice aged 3 weeks *KCNQ2*$^{WT/WT}$ (n = 70 cells, 3 animals), *KCNQ2*$^{WT/T274M}$ (n= 46 cells, 2 animals).

Figure 7: Measurement of the length of the AIS and AIS-soma distance in pyramidal cells of layer V in motor cortical slices from developing *KCNQ2*$^{WT/WT}$ and *KCNQ2*$^{WT/T274M}$ mice.

A) Graphs show the quantification of the AIS length (right) and of the AIS-soma distance (left) in individual cells from *KCNQ2*$^{WT/WT}$ mice aged (black dots, n = 60 cells, 3 animals) and *KCNQ2*$^{WT/T274M}$ mice (red squares, n= 59 cells, 3 animals) aged one week. Larger symbols are the mean (± S.E.M) of

the values from the 2 groups of mice. **B**) Same quantification in cells from mice aged three weeks. *KCNQ2*$^{WT/WT}$ (n = 32 cells, 2 animals), *KCNQ2*$^{WT/T274M}$ (n= 11 cells, 1 animal); **C)** Quantification in cells from mice aged 5 weeks *KCNQ2*$^{WT/WT}$ (n = 95 cells, 3 animals), *KCNQ2*$^{WT/T274M}$ (n= 79 cells, 3 animals).

Figure 8: Recurrent GABAergic network activity in motor cortical slices

A) Upper trace: pyramidal cell of the layer II/III from a *KCNQ2*$^{WT/T274M}$ mouse aged 3 weeks and recorded in cell attached configuration. Lower traces: same cell recorded in whole cell configuration. The spontaneous activity is characterized by the presence of recurrent large outward current reversing polarity at -70 mV and which frequency is insensitive to the membrane potential. **B)** Other pyramidal cell of the layer II/III from a *KCNQ2*$^{WT/T274M}$ mice aged 3 weeks and recorded in cell attached configuration (note the presence of small oscillation of the current) and in whole cell configuration. The traces show RGNA recorded in control, in the presence of NBQX 10 µM and D-APV (40 µM), and in the presence of gabazine (5 µM).

Figure 9: Effect of the p.T274M variant on spontaneous activities recorded in pyramidal cells of the layer II/III

A) Representative traces showing spontaneous activities recorded at 0 mV and -70 mV in pyramidal cells of the layer II/III in motor cortical slices from *KCNQ2*$^{WT/WT}$ (black traces) and *KCNQ2*$^{WT/T274M}$ (blue traces) mice aged one week (PND 7-9). RGNA are recorded at 0 mV, GluR- PSC are recorded at -70 mV. Graphs below show the quantification (mean ± S.E.M) of the number of cells in which RGNA were observed, the frequency of RGNA, the charge transfer during RGNA, the total frequency of spontaneous GABAR-mediated post-synaptic currents (events in and out RGNA) recorded at 0 mV and the frequency of GluR-mediated post-synaptic currents recorded at -70 mV. Black: wild type cells (n = 17, 3 animals); blue: mutant cells (n = 19, 4 animals). **B)** Same quantification in cells from mice aged three weeks (PND19-21). Wild-type cells (n = 19 cells, 5 animals), mutant cells (n = 19 cells, 4 animals). **C)** Same quantification in cells from mice aged 4-5 weeks (PND 28-35). RGNA were not observed (NA, not available). Wild type cells (n= 14 cells, 2 animals), mutant cells (n =14 cells, 2 animals). Statistics: * $p< 0.05$; ** : $p< 0.01$; ***$p<0.001$.

Figure 10: Effect of the p.T274M variant on spontaneous activities recorded in pyramidal cells of the layer V

A) Quantification (mean ± S.E.M) of the number of cells in which RGNA were observed, the frequency of RGNA, the charge transfer during RGNA, the total frequency of spontaneous GABAR-mediated post-synaptic currents (GABAR-PSC, events in and out RGNA) recorded at 0 mV and the frequency of GluR-mediated post-synaptic currents (GluR-PSC) recorded at -70 mV. Black: wild type cells (n = 14, 4 animals); red: mutant cells (n = 14, 3 animals). **B)** Same quantification in cells from

mice aged three weeks (PND19-21). Wild-type cells (n = 14 cells, 3 animals), mutant cells (n = 18 cells, 4 animals). **C)** Same quantification in cells from mice aged 4-5 weeks (PND 28-35). RGNA were not observed (NA, not available). Wild type cells (n= 13 cells, 2 animals), mutant cells (n =12 cells, 2 animals). Statistics: * $p< 0.05$; ** : $p< 0.01$; ***$p<0.001$.

Figure 1

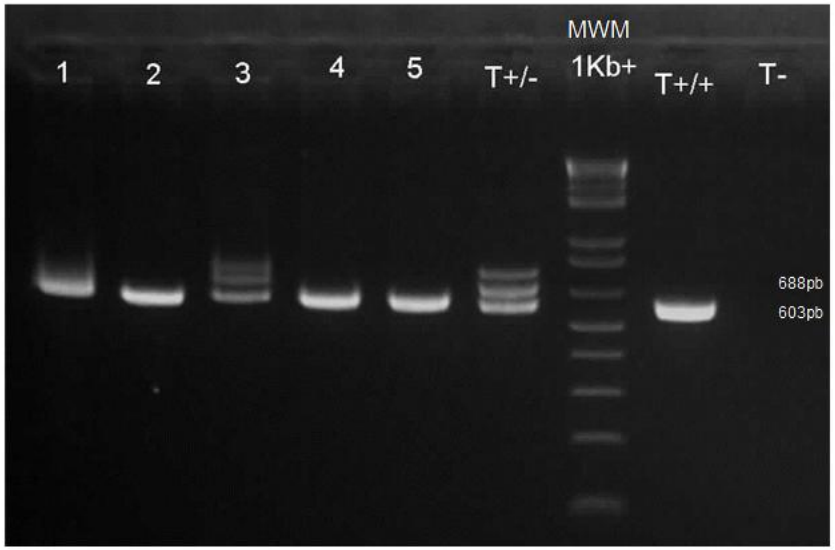

Figure 2

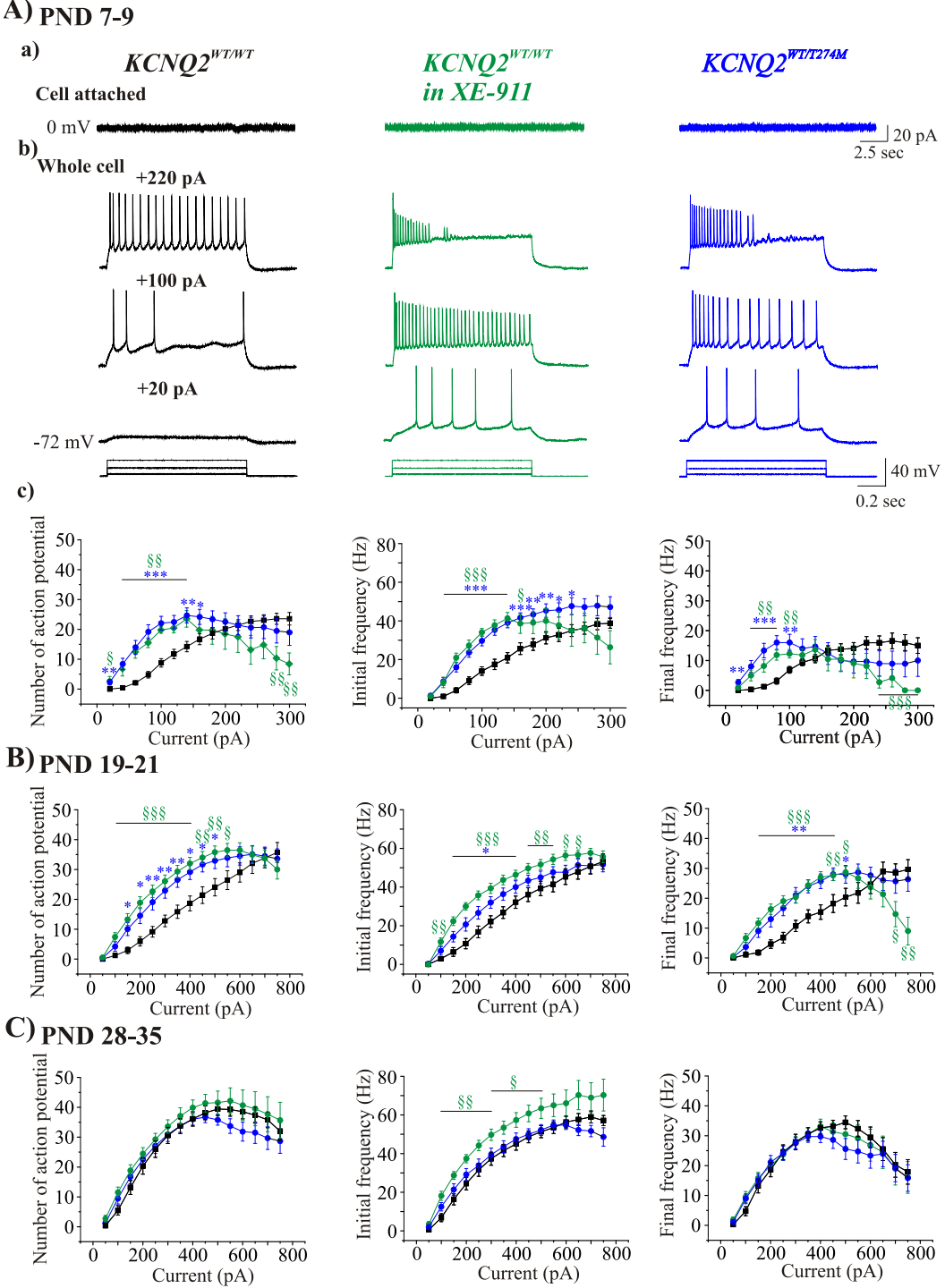
A) PND 7-9
a)
KCNQ2WT/WT
KCNQ2WT/WT in XE-911
KCNQ2WT/T274M
Cell attached
0 mV
20 pA
2.5 sec
b)
Whole cell
+220 pA
+100 pA
+20 pA
-72 mV
40 mV
0.2 sec
c)
Number of action potential
Initial frequency (Hz)
Final frequency (Hz)
Current (pA)
B) PND 19-21
C) PND 28-35

Figure 3

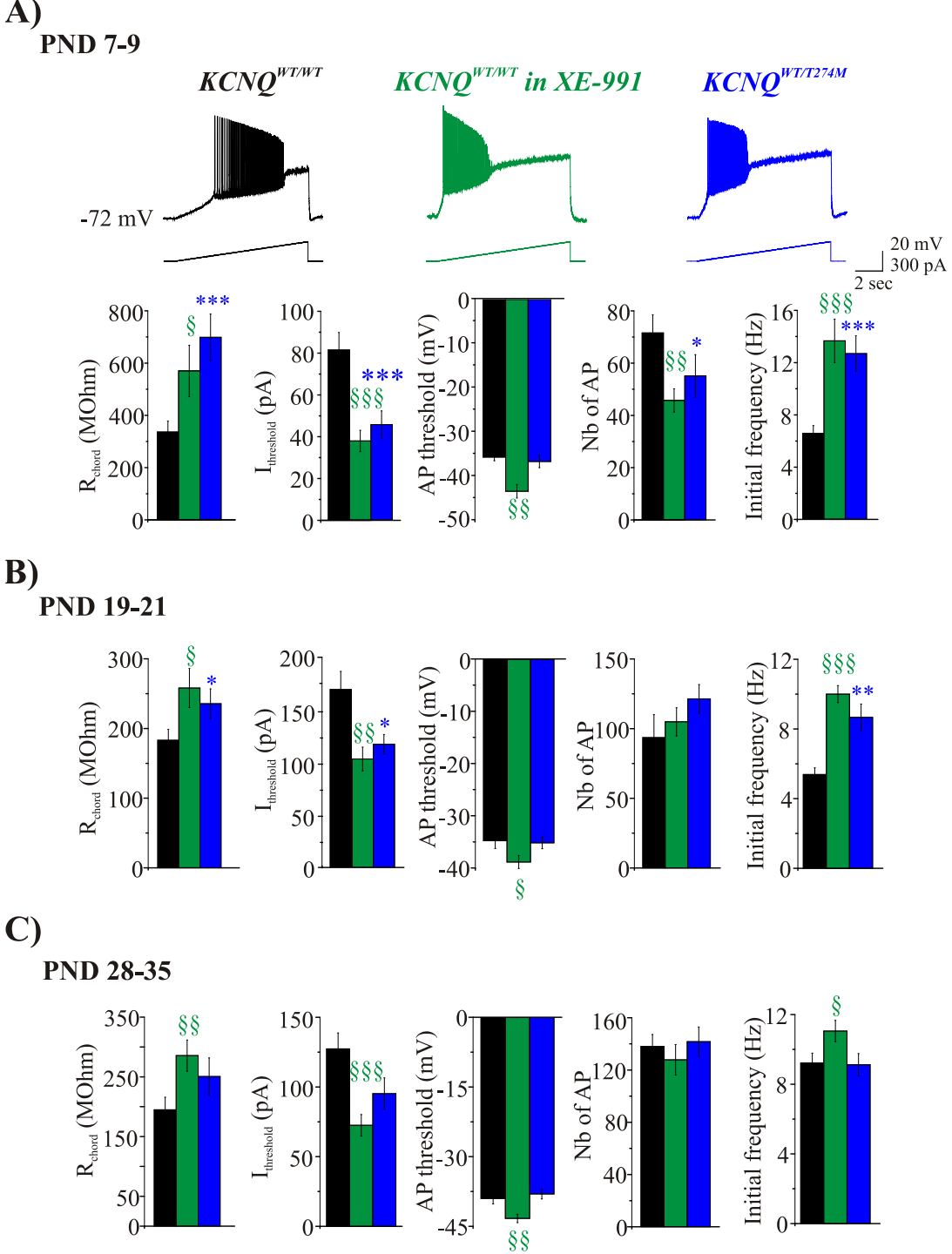
A)
PND 7-9
KCNQ^WT/WT
KCNQ^WT/WT in XE-991
KCNQ^WT/T274M
-72 mV
20 mV
300 pA
2 sec
R_chord (MOhm)
I_threshold (pA)
AP threshold (mV)
Nb of AP
Initial frequency (Hz)
B)
PND 19-21
C)
PND 28-35

Figure 4

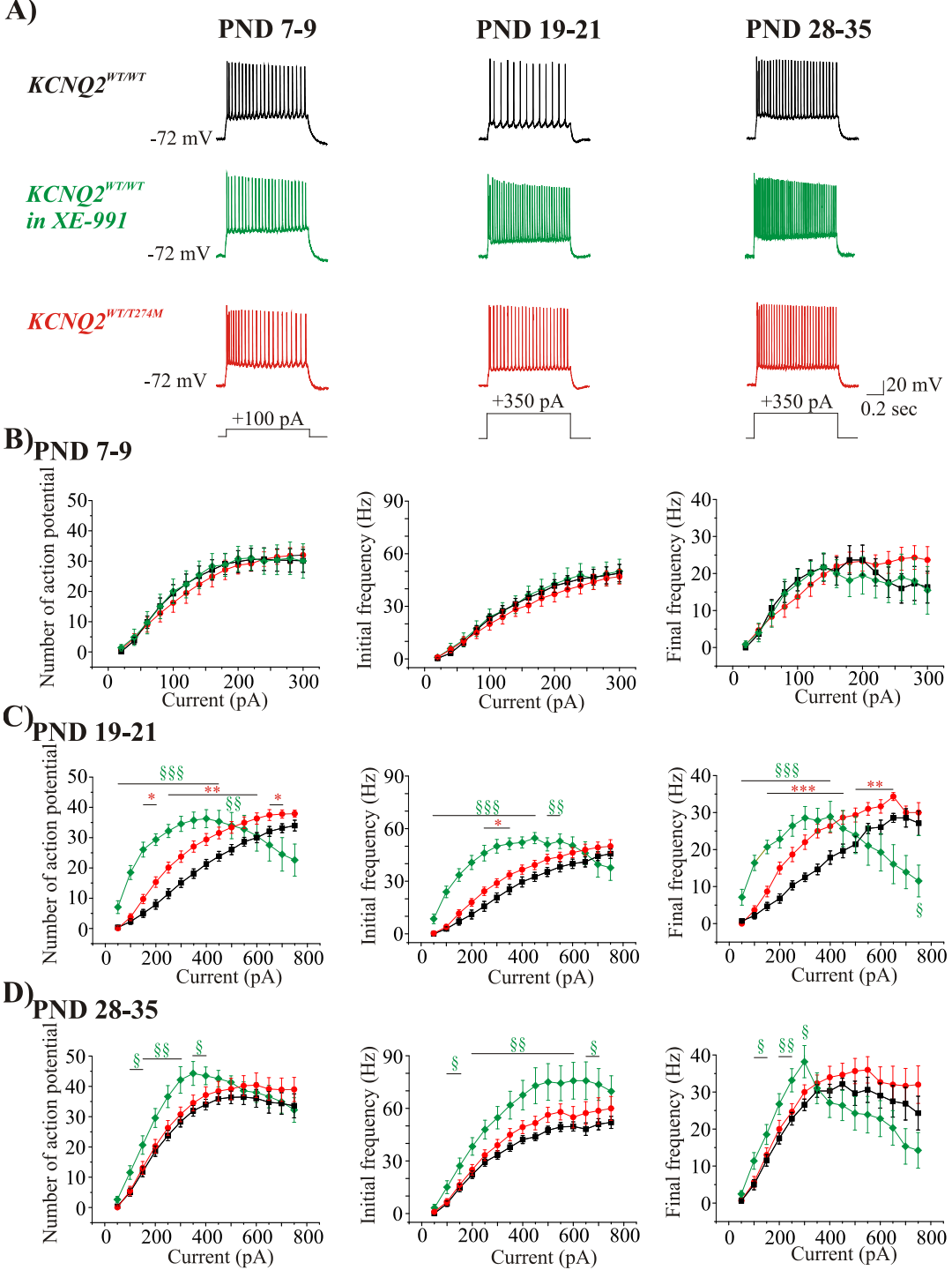
A)
PND 7-9
PND 19-21
PND 28-35
KCNQ2WT/WT
-72 mV
KCNQ2WT/WT
in XE-991
-72 mV
KCNQ2WT/T274M
-72 mV
+100 pA
+350 pA
+350 pA
20 mV
0.2 sec
B) PND 7-9
C) PND 19-21
D) PND 28-35
Number of action potential
Initial frequency (Hz)
Final frequency (Hz)
Current (pA)

Figure 5

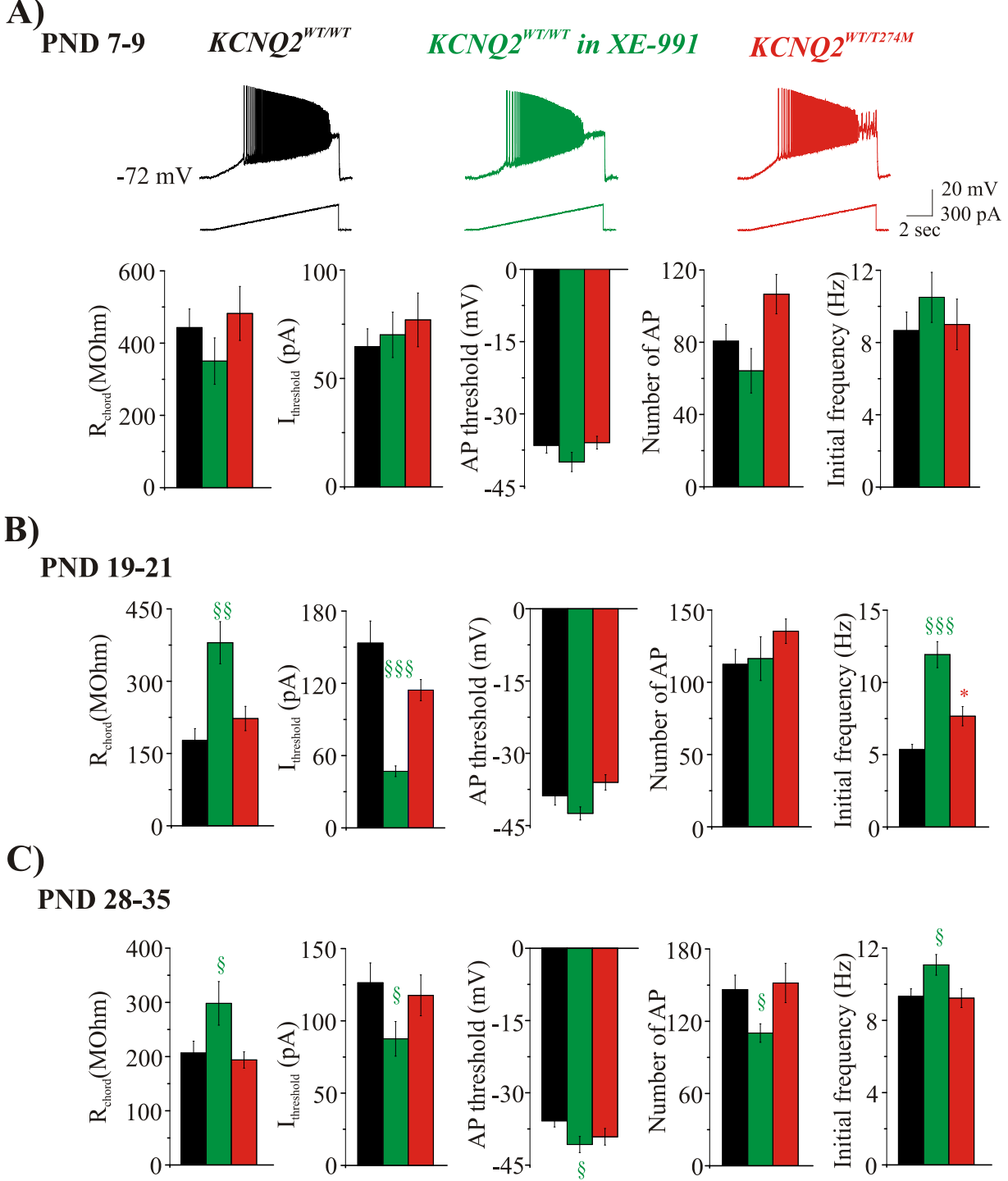
A)
PND 7-9
KCNQ2WT/WT
KCNQ2WT/WT in XE-991
KCNQ2WT/T274M
-72 mV
20 mV
300 pA
2 sec
Rchord(MOhm)
Ithreshold (pA)
AP threshold (mV)
Number of AP
Initial frequency (Hz)
B)
PND 19-21
C)
PND 28-35
§
§§
§§§
*

Figure 6

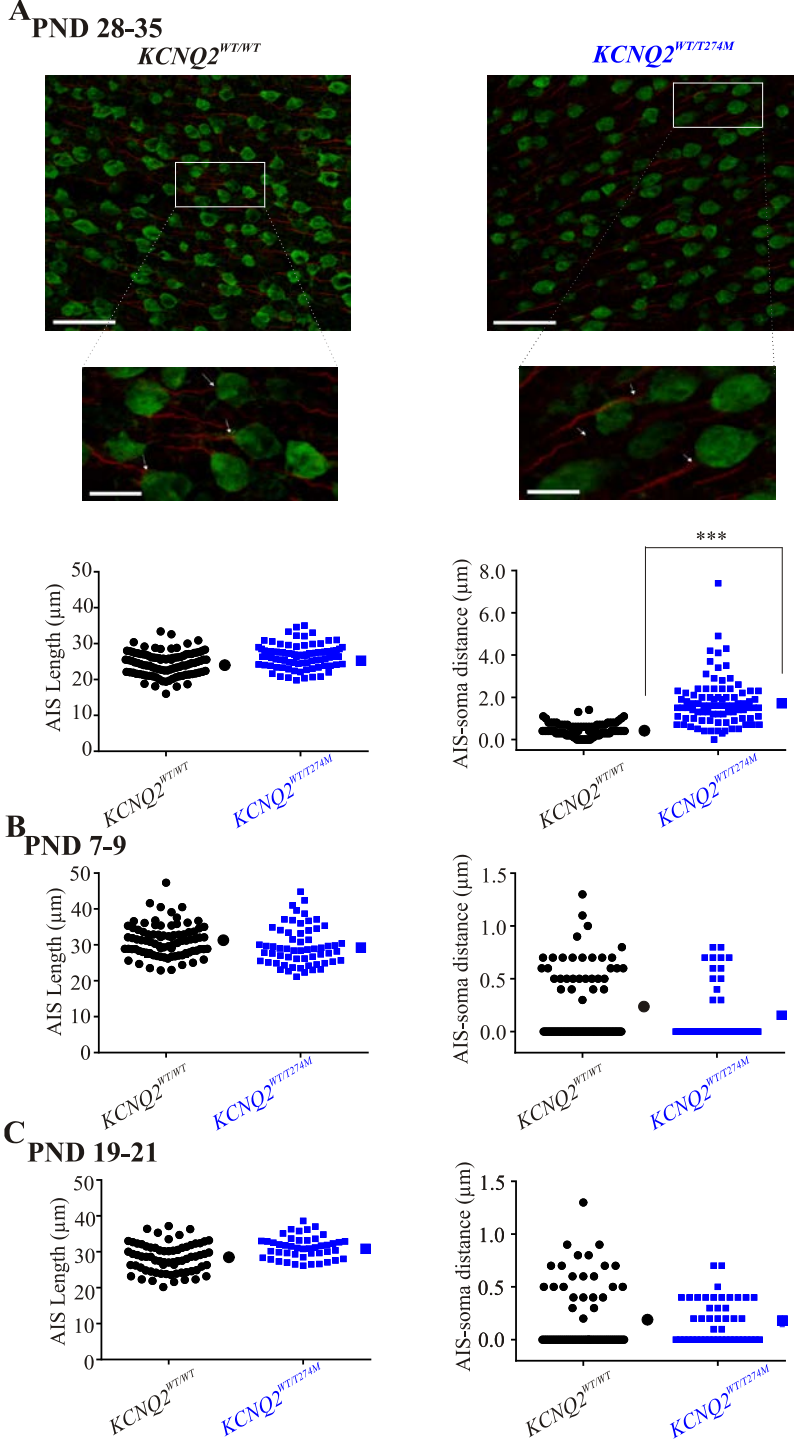
A
PND 28-35
KCNQ2WT/WT
KCNQ2WT/T274M
AIS Length (µm)
AIS-soma distance (µm)
***
B
PND 7-9
C
PND 19-21

Figure 7

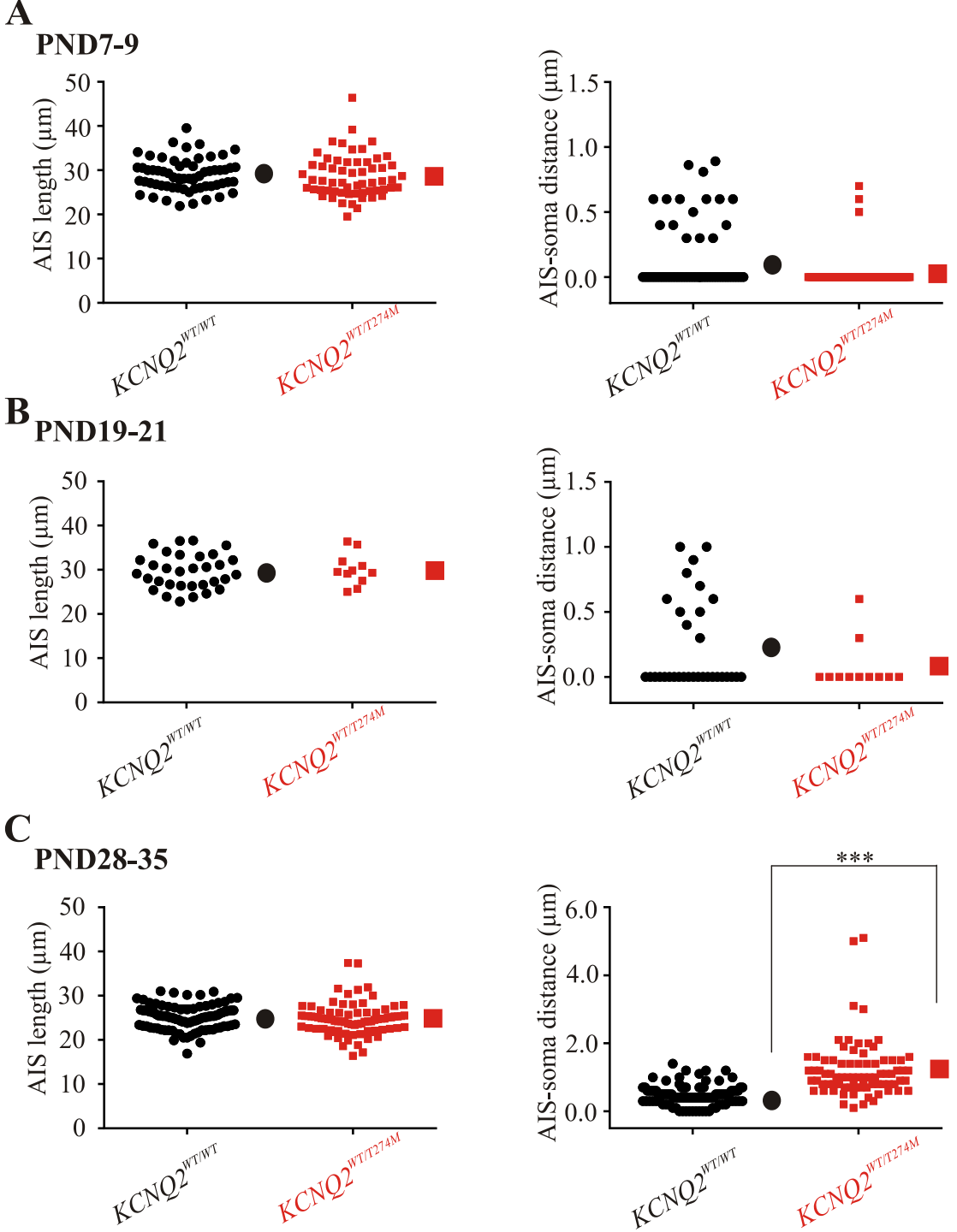
A
PND7-9
AIS length (μm)
AIS-soma distance (μm)
B
PND19-21
AIS length (μm)
AIS-soma distance (μm)
C
PND28-35
AIS length (μm)
AIS-soma distance (μm)
***
KCNQ2WT/WT
KCNQ2WT/T274M

Figure 8

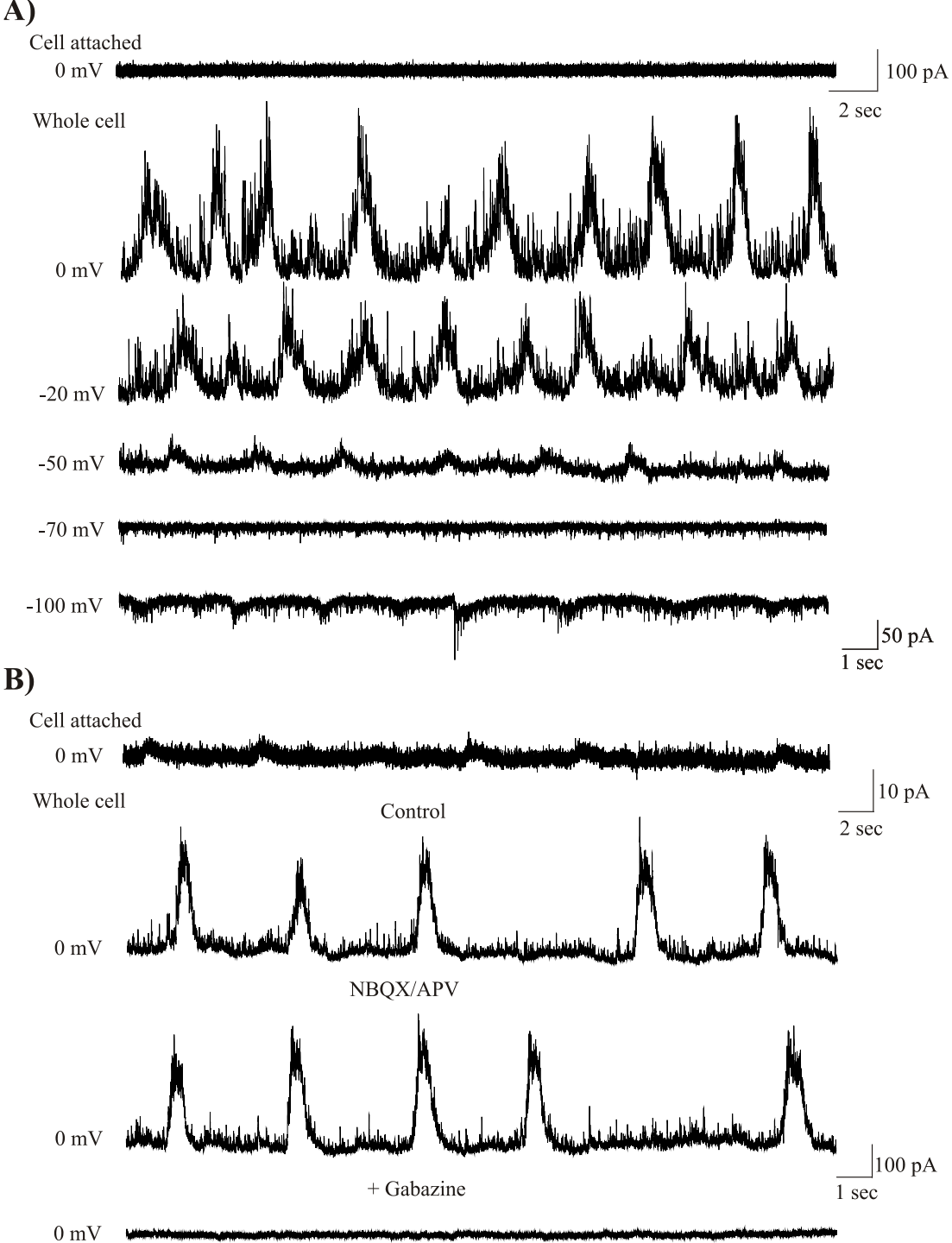
A)
Cell attached
0 mV
100 pA
2 sec
Whole cell
0 mV
-20 mV
-50 mV
-70 mV
-100 mV
50 pA
1 sec
B)
Cell attached
0 mV
10 pA
2 sec
Whole cell
Control
0 mV
NBQX/APV
0 mV
100 pA
1 sec
+ Gabazine
0 mV

Figure 9

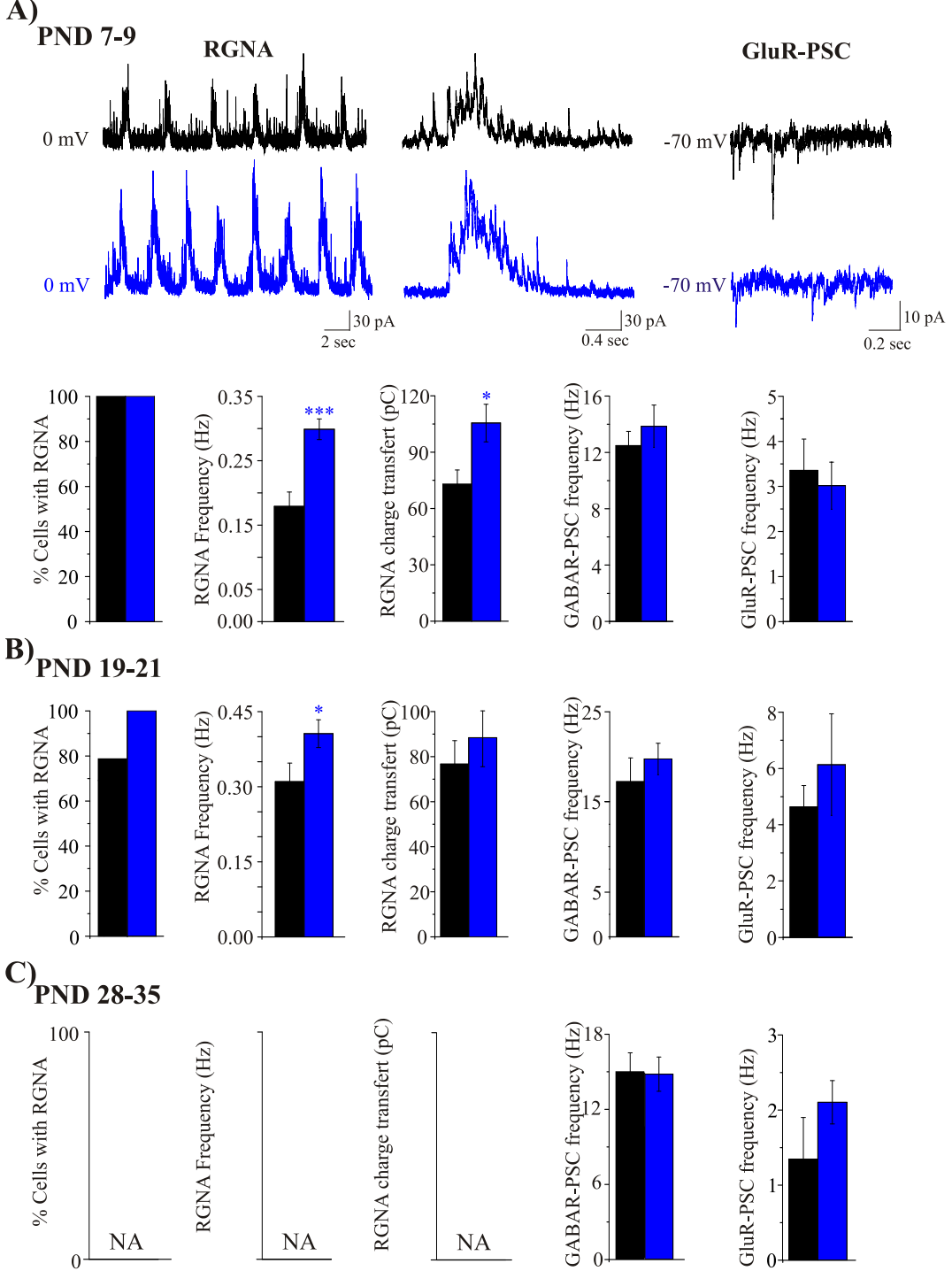
A)
PND 7-9
RGNA
GluR-PSC
0 mV
0 mV
-70 mV
-70 mV
30 pA
2 sec
30 pA
0.4 sec
10 pA
0.2 sec
% Cells with RGNA
RGNA Frequency (Hz)
***
RGNA charge transfert (pC)
*
GABAR-PSC frequency (Hz)
GluR-PSC frequency (Hz)
B)
PND 19-21
*
C)
PND 28-35
NA
NA
NA

Figure 10

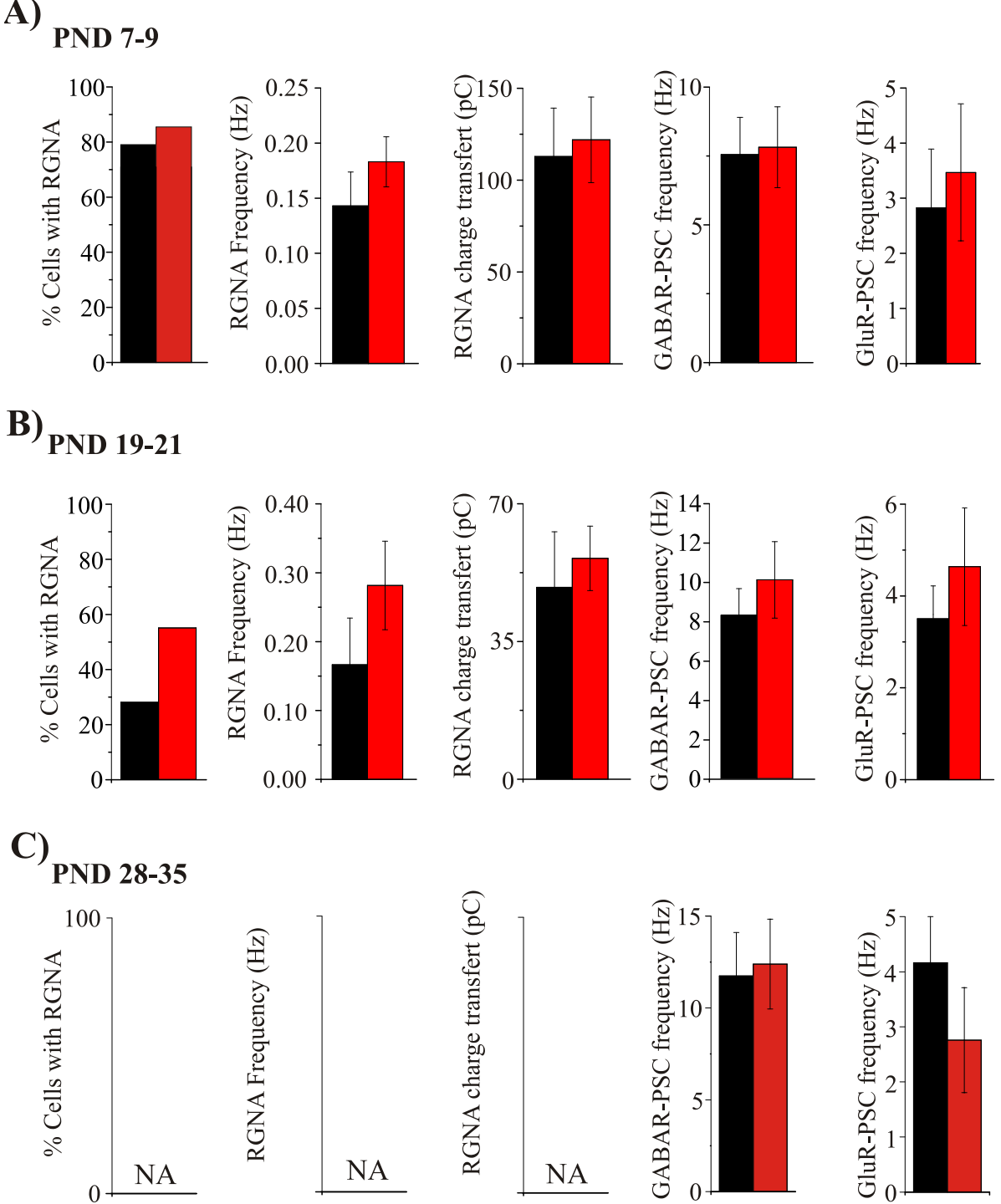
A)
PND 7-9
% Cells with RGNA
RGNA Frequency (Hz)
RGNA charge transfert (pC)
GABAR-PSC frequency (Hz)
GluR-PSC frequency (Hz)
B)
PND 19-21
% Cells with RGNA
RGNA Frequency (Hz)
RGNA charge transfert (pC)
GABAR-PSC frequency (Hz)
GluR-PSC frequency (Hz)
C)
PND 28-35
% Cells with RGNA
NA
RGNA Frequency (Hz)
NA
RGNA charge transfert (pC)
NA
GABAR-PSC frequency (Hz)
GluR-PSC frequency (Hz)